

Microscopic description of fission in odd-mass uranium and plutonium nuclei with the Gogny energy density functional

R. Rodríguez-Guzmán¹ and L. M. Robledo^{2,3}

¹ *Physics Department, Kuwait University, Kuwait 13060, Kuwait.*

² *Departamento de Física Teórica, Universidad Autónoma de Madrid, 28049-Madrid, Spain*

³ *Center for Computational Simulation, Universidad Politécnica de Madrid, Campus de Montegancedo, Boadilla del Monte, 28660-Madrid. Spain*

(Dated: March 24, 2022)

The parametrization DIM of the Gogny energy density functional is used to study fission in the odd-mass Uranium and Plutonium isotopes with $A=233, \dots, 249$ within the framework of the Hartree-Fock-Bogoliubov (HFB) Equal Filling Approximation (EFA). Ground state quantum numbers and deformations, pairing energies, one-neutron separation energies, barrier heights and fission isomer excitation energies are given. Fission paths, collective masses and zero point rotational and vibrational quantum corrections are used to compute the systematic of the spontaneous fission half-lives t_{SF} , the masses and charges of the fission fragments as well as their intrinsic shapes. Although there exists a strong variance of the predicted fission rates with respect to the details involved in their computation, it is shown that both the specialization energy and the pairing quenching effects, taken into account fully variationally within the HFB-EFA blocking scheme, lead to larger spontaneous fission half-lives in odd-mass U and Pu nuclei as compared with the corresponding even-even neighbors. It is shown that modifications of a few percent in the strengths of the neutron and proton pairing fields can have a significant impact on the collective masses leading to uncertainties of several orders of magnitude in the predicted t_{SF} values. Alpha-decay lifetimes have also been computed using a parametrization of the Viola-Seaborg formula.

PACS numbers: 24.75.+i, 25.85.Ca, 21.60.Jz, 27.90.+b, 21.10.Pc

I. INTRODUCTION.

Fission is one of the many possible decay modes of heavy atomic nuclei [1, 2] and, due to its characteristics, has attracted considerable attention since its discovery. It can be viewed [3] as the result of the competition between the nuclear surface energy, coming from the short range character of the strong nuclear interaction, and the Coulomb repulsion among protons. On the way to scission, atomic nuclei exhibit pronounced shape changes consequence of the subtle balance between Coulomb, surface energy and quantum shell effects associated to the underlying single particle structure of atomic nuclei. Fission is then portrayed as a phenomenon where the shape of the nucleus, described in terms of several deformation parameters, evolves from the ground state to scission [1, 2, 4–6]. How to account for those shape changes, and the associated quantum shell effects, still remains a major challenge in modern nuclear structure physics [5, 6] with an impact on both basic research and technology.

A better knowledge of the fission process is required, for example, to deepen our understanding of the survival chances of a given element as one goes up in atomic number Z [5, 7–10], to account for the competition between different decay modes (fission, α -decay, cluster radioactivity, ...) [11–18] and to disentangle its role in the r -process [19–21]. Furthermore, fission is of high interest for the already existing and the new generation of nuclear reactors, the radioactive waste problem, weapon tests and the production of super-heavy elements (see, for example, [2, 4, 22–24] and references therein).

Among the several theoretical frameworks used in fission studies, the (constrained) mean-field [25] approximation has emerged as a powerful tool. Here, the Hartree-Fock-Bogoliubov (HFB) method with constraints on multipole moments, necking operators, etc is used to compute a multidimensional energy landscape defining the potential energy to be used in fission dynamics [5, 6]. Each configuration in the fission landscape of a given even-even nucleus is usually labeled by a set of shape deformation parameters like the quadrupole, octupole, ... multipole moments, referred to collectively as $\mathbf{Q}=(Q_{20}, Q_{30}, \dots)$. On the other hand, the mean-field framework also provides, in a unified manner, the collective inertias as well as the zero-point quantum rotational and vibrational energy corrections [13] which are the required ingredients to describe the quantum mechanical tunneling effect through the fission barrier. With these basic ingredients it is possible to make theoretical predictions about the spontaneous fission half-lives t_{SF} and other relevant observable [6, 13–15, 17, 26]. The mean field description of fission requires an effective energy density functional (EDF). Popular choices are the non-relativistic Gogny [8, 9, 13–15, 26–30], Skyrme [31–35], Barcelona-Catania-Paris-Madrid (BCPM) [17, 36] and relativistic [37–40] EDFs.

In spite of the progress made in recent years in the study of the properties of odd-mass nuclei [41–49], a task greatly facilitated by developments in high-performance computing, microscopic fission studies in those nuclear systems are still rather scarce within the EDF framework. This is mainly due to major technical difficul-

ties [16] that appear in the description of odd nuclei, as compared to their even-even counterparts. First, to describe an odd-mass nucleus time-reversal-breaking one-quasiparticle "blocked" wave functions [25] should be used. Therefore, time-odd fields should be computed which increasing by a factor of two the computing time required for the solution of the mean-field equations. Second, several one-quasiparticle initial states have to be considered for each configuration in the multidimensional energy landscape in order to reach the lowest energy solution as the self-consistent character of the HFB equation does not guarantee to obtain the lowest-energy solution by blocking the lowest one-quasiparticle state. Third, reorientation effects [49, 50] should also be taken into account in the solution of the mean-field equations. Therefore, an approximation is required to reduce the computational effort in EDF fission studies for heavy odd-mass systems. Within this context, the Equal Filling Approximation (EFA) [42–48, 51] represents a reasonable alternative to the full fledged HFB plus blocking procedure [16]. The Hartree-Fock-Bogoliubov EFA (HFB-EFA) has already been formulated in a fully Ritz-variational fashion [42] by introducing a quantum statistical ensemble where the one-quasiparticle configuration μ to be "blocked" and its Kramer's partner $\bar{\mu}$ have the same probability (1/2). Under this assumption, time-reversal invariance is preserved and only time-even fields have to be considered in the solution of the HFB equation. Let us stress that one of the main advantages of the variational formulation of the HFB-EFA is that it allows the use of the standard gradient method [52] to solve the system of mean-field equations, with the subsequent simplification in the treatment of many constraints at the same time [45–48].

One of the most prominent experimental features in heavy odd-mass nuclei is their larger spontaneous fission half-lives as compared with their even-even counterparts [1, 2, 53]. In order to explain such a feature two mechanisms have been invoked in the literature, namely, the so called specialization energy [54] and the quenching of pairing correlations. The specialization energy modifies the collective potential felt by the odd-mass nucleus on its way to scission making the inner fission barrier height higher than in the corresponding even-even case. It essentially arises from the assumption that the K quantum number, i.e., the projection of the angular momentum along the intrinsic nuclear axial symmetry axis, should be conserved along the fission process [16, 54]. On the other hand, in an odd-mass system, pairing correlations are quenched by the unpaired nucleon and there is a weakening of the strength of the pairing field [25]. As the collective inertias exhibit a strong dependence on the inverse of the square of the pairing gap [13–15, 17, 55, 56] the weakening of pairing correlations in an odd system leads to a bigger collective inertia and therefore to an enhancement of the collective action. As a consequence, the spontaneous fission life time t_{SF} values take bigger values in the odd-A system than in the neighboring even-even nuclei [16].

Recently, the fission properties of $^{251,253,255,257,259}\text{No}$ [16] have been evaluated within the HFB-EFA scheme. Our calculations provide a reasonable account of the ground state quantum numbers and deformations, pairing energies, one-neutron separation energies, excitation energies of fission isomers as well as the inner and outer barrier heights. For those nuclei, we have also studied the systematic of the spontaneous fission and α -decay lifetimes. Though there exists a strong variance of the predicted fission rates with respect to the details involved in their computation, it has been shown that both the specialization energy and the quenching of pairing correlations, taken into account selfconsistently within the HFB-EFA blocking procedure, lead to larger t_{SF} values in odd-mass No isotopes as compared with their even-even neighbors [53].

In this paper we consider the fission properties of odd-mass neutron-rich uranium and plutonium nuclei within the (constrained) HFB-EFA [16, 42, 45–48] based on the parametrization D1M [57] of the non-relativistic Gogny-EDF [58]. Previous studies for even-even [59–62] and also for odd-mass [16, 45–48] nuclei have shown that the parametrization D1M of the Gogny force preserves the predictive power of the well tested and well-performing Gogny-D1S [27] EDF while improving the description of nuclear masses [57]. In particular, previous calculations [13–16] reveal that the Gogny-D1M EDF represents a reasonable starting point to describe fission properties in heavy and super-heavy nuclear systems. In this work we have employed the Gogny-D1M HFB-EFA, for the first time, to study the fission properties of odd-A U and Pu isotopes with $A=233, \dots, 249$ taken as illustrative samples. One should keep in mind that a better knowledge of the fission properties of neutron-rich nuclei is required as these are the territories where the fate of the nucleosynthesis of heavy elements is determined [19–21].

The paper is organized as follows: in Sec. II, we briefly outline the HFB-EFA [42] method as well as the methodology employed to obtain the one (1F) and two-fragment (2F) fission paths. We also discuss the relevant details regarding the computation of the spontaneous fission t_{SF} and α -decay t_α lifetimes. The results of our calculations are discussed in Sec. III. First, in Sec. III A, we illustrate our methodology in the case of ^{243}U . The same methodology has been employed for all the other odd-mass nuclei considered in this work. The systematic of the fission paths, spontaneous fission half-lives as well as fragment mass and charge is presented in Sec. III B. In Sec. III C, we discuss the impact of pairing correlations on the predicted spontaneous fission half-lives. To this end, we have also considered the Gogny-D1M EDF though with the strengths of the proton and neutron pairing fields increased by 5 and 10 % to simulate effects of dynamical pairing that could appear as a consequence of symmetry restoration and/or a dynamical description of fission. For the sake of completeness, we will also include in the corresponding figures results already obtained for even-even U and Pu nuclei [13, 14]. Finally, Sec. IV is de-

voted to the concluding remarks and work perspectives.

II. THEORETICAL FRAMEWORK

In this section, we briefly outline the theoretical framework used in this study, i.e., the (constrained) HFB-EFA method used with the parametrization D1M of the Gogny-EDF. The reader is referred to Ref. [42] for a theoretical justification of the HFB-EFA based on ideas of quantum statistical mechanics. We also describe the methodology employed to obtain the fission paths in the studied odd-mass nuclei. Finally, we present the relevant details regarding the computation of the spontaneous fission t_{SF} and α -decay t_α lifetimes.

In the HFB-EFA formalism the density matrix $\rho_{ij}^{(\mu, EFA)}$ and pairing tensor $\kappa_{ij}^{(\mu, EFA)}$ take the form

$$\begin{aligned} \rho_{ij}^{(\mu, EFA)} &= (V^*V^T)_{ij} + \frac{1}{2} (U_{i\mu}U_{j\mu}^* - V_{i\mu}^*V_{j\mu}) \\ &+ \frac{1}{2} (U_{i\bar{\mu}}U_{j\bar{\mu}}^* - V_{i\bar{\mu}}^*V_{j\bar{\mu}}) \end{aligned} \quad (1)$$

and

$$\begin{aligned} \kappa_{ij}^{(\mu, EFA)} &= (V^*U^T)_{ij} + \frac{1}{2} (U_{i\mu}V_{j\mu}^* - V_{i\mu}^*U_{j\mu}) \\ &+ \frac{1}{2} (U_{i\bar{\mu}}V_{j\bar{\mu}}^* - V_{i\bar{\mu}}^*U_{j\bar{\mu}}) \end{aligned} \quad (2)$$

where, the one-quasiparticle configuration, labeled by the index μ , and its Kramers' partner $\bar{\mu}$ have the same occupancies $n_\mu = n_{\bar{\mu}} = 1/2$. In the above expression the U and V matrices represent the amplitudes of the Bogoliubov transformation, according to the standard notation of Ref [25]. The above expressions of the density matrix and pairing tensor are the ones of an statistical ensemble with two species (the blocked configurations μ and $\bar{\mu}$) both with probability 1/2. Thanks to Gaudin's theorem [63, 64] (the equivalent of Wick's theorem but for statistical ensembles), the mean value of any observable in such a statistical ensemble takes the same form as in standard HFB but replacing the densities by the ones of Eqs (1) and (2). This is the basic assumption of the EFA. Moreover, the Ritz variational principle applied to the total energy, written as a functional of both $\rho_{ij}^{(\mu, EFA)}$ and $\kappa_{ij}^{(\mu, EFA)}$ leads to the standard HFB-EFA equation. As a consequence of its variational nature the HFB-EFA equation can be solved using the successful gradient method [52].

In our calculations we assume axial symmetry and therefore we can use the K quantum number (projection along the symmetry axis of the angular momentum) to label the one-quasiparticle excitations. On the other hand, reflection symmetry is allowed to break as required by the physics of mass asymmetric fission. As a consequence parity might not a good quantum number along the whole fission path. The Gogny D1M EDF

has been used in the calculation with the standard assumptions: the two body kinetic energy correction is fully taken into account, the Coulomb exchange contribution to the energy is treated in the Slater approximation [65] and Coulomb antipairing is fully neglected. As reflection symmetry is broken, an additional constraint on the center of mass is used to avoid spurious center of mass effects [59, 60]. Finally, the traditional zero-point rotational energy correction $\Delta E_{ROT} = \langle \Delta \hat{J}^2 \rangle / \mathcal{J}_{Yocc}$ as well as the vibrational one have been added *a posteriori* to the HFB energies [13–15].

As mentioned before, reaching the lowest energy solutions for each K quantum number requires the use of several initial configurations. In the following we describe the methodology employed in this study to deal with this and other peculiarities of odd mass nuclei. We will use ^{243}U (see, Sec. III A) as an illustrative example.

Step 1) Determination of the 1F and 2F solutions for the even-even neighbor ^{242}U within the constrained HFB framework. Those wave functions have been computed using the same methodology and (optimized) axially symmetric harmonic oscillator basis as in Ref. [13]. We have employed constraints on the axially symmetric quadrupole \hat{Q}_{20} and octupole \hat{Q}_{30} operators [59, 60] to obtain the 1F solutions. For sufficiently large quadrupole moments, 2F solutions have been reached by constraining on the necking operator $\hat{Q}_{Neck}(z_0, C_0) = \exp(-(z - z_0)^2/C_0^2)$ used to fix the number of particles in a region around z_0 of width C_0 [13–15].

Step 2) Determination of the "average" 1F and 2F solutions for ^{243}U within the constrained HFB framework. We have used the 1F and 2F solutions obtained for ^{242}U (Step 1) as initial wave functions to compute "average" (AV) 1F and 2F solutions, respectively, for ^{243}U (see, Fig. 1). Calculations have been carried out as for an even-even nucleus (i.e., no blocking is performed and all wave functions with even number parity) but, with the mean value of the neutron number operator constrained to be $\langle \hat{N} \rangle = 151$. We have employed the (optimized) HO basis resulting from Step 1. The zero-point quantum energy corrections have also been added *a posteriori* to the HFB energies.

Step 3) Identification of the (ground-state) $K = K_0$ quantum number for ^{243}U within the HFB-EFA. We have carried out HFB-EFA blocking calculations starting from the wave function corresponding to the absolute minimum of the AV 1F path (Step 2) in ^{243}U . We have repeated the blocking procedure, using the same HO basis as in Step 2, several times so as to obtain five different solutions of the HFB-EFA equations for each of the values of K from 1/2 up to 11/2. Larger K values have not been taken into account as the neutron single-particle levels corresponding to them are too far from the Fermi surfaces. We have then identified, the $K = K_0$ quantum number corresponding to the lowest energy (i.e., the ground state) among all the K -solutions obtained for ^{243}U .

Step 4) Determination of the 1F and 2F K_0 -solutions

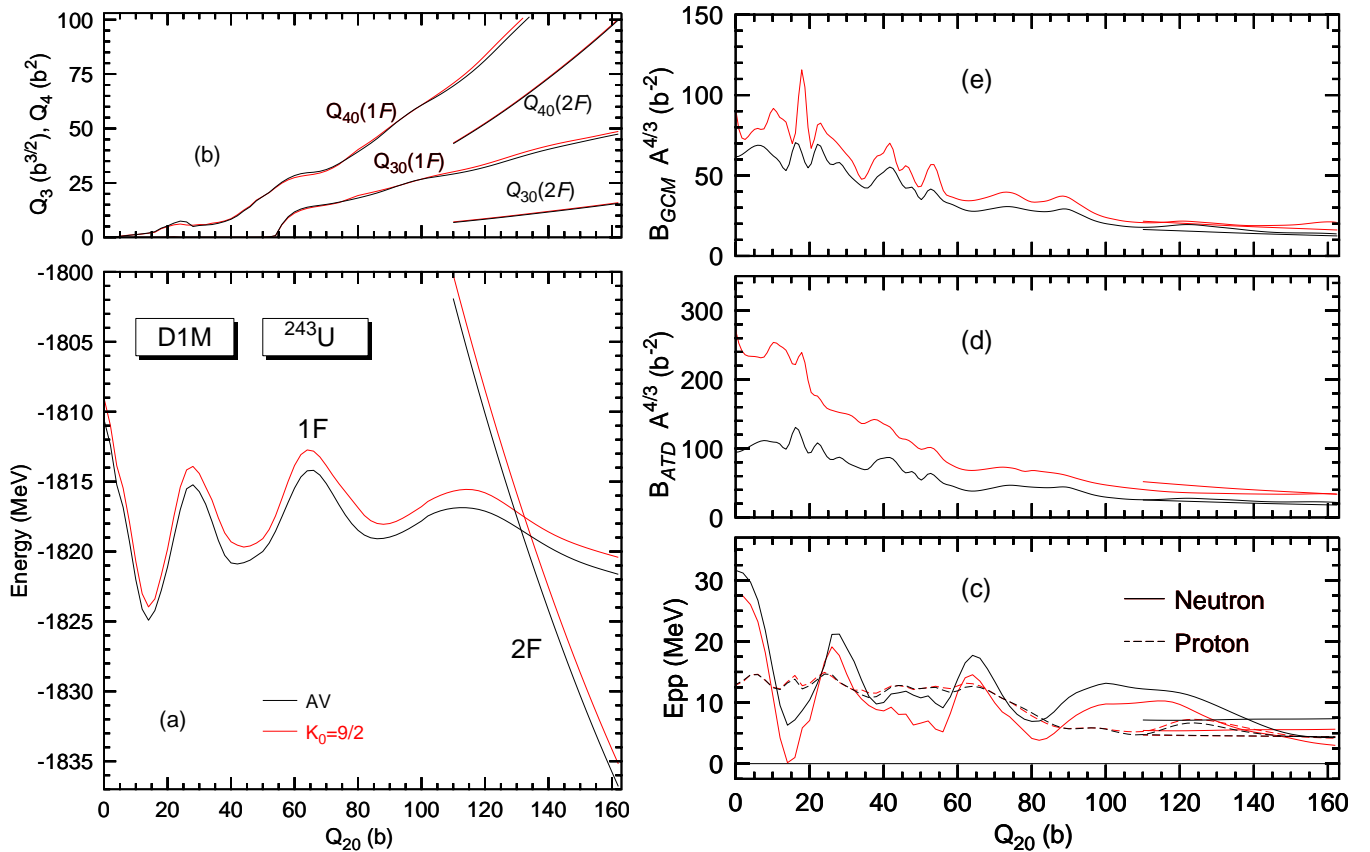


FIG. 1: (Color online) The $K_0 = 9/2$ HFB-EFA plus the zero point rotational energies, are plotted in panel (a) as functions of the quadrupole moment Q_{20} for the nucleus ^{243}U . Both the one (1F) and two-fragment (2F) solutions are included in the plot. The octupole Q_{30} and hexadecapole Q_{40} moments corresponding to the 1F and 2F solutions are shown in panel (b). The pairing interaction energies are depicted in panel (c) for protons (dashed lines) and neutrons (full lines). The collective ATD and GCM masses are plotted in panels (d) and (e), respectively. Results corresponding to "average" (AV) HFB calculations for ^{243}U have also been included in each panel. For more details, see the main text.

for ^{243}U within the constrained HFB-EFA. Having the corresponding AV 1F and 2F wave functions (Step 2) and the ground state quantum number K_0 for ^{243}U , we have computed 1F and 2F K_0 -solutions, respectively. Note, that we are assuming that the spontaneous fission of ^{243}U will take place in a configuration with the same $K = K_0$ value as the one of the ground state [16, 54]. However, parity can be broken along the fission path. For each AV 1F and/or 2F state, we have repeated the blocking procedure, using the same HO basis as in Step 2, several times so as to obtain five different solutions of the HFB-EFA equations with the same $K=K_0$ value. This is the most time consuming step in our calculations as we move all over the AV 1F and 2F paths performing the required K_0 -blocking for each \mathbf{Q} -configuration. This, already substantial, computational effort is greatly helped by the combined use of the HFB-EFA [42] and the gradient method to solve its equations [52]. The 1F and 2F K_0 -solutions with the lowest energy, for each \mathbf{Q} -configuration, are the ones used to build the ground state fission path for ^{243}U (see, Fig. 1).

The rotational energy correction ΔE_{ROT} to the HFB-

EFA energies have been computed in terms of the Yoccoz moment of inertia using the formulas for even-even nuclei [16, 66–68]. The reason for this choice is that an approximate angular momentum projection, like the one leading to the rotational energy correction, has not yet been carried out within the HFB-EFA. Work along these lines is in progress and will be reported elsewhere. On the other hand, previous finite temperature Adiabatic Time Dependent (ATD) results [69–71] can be extended to the HFB-EFA via its statistical density matrix operator [42]. This, in turn, allows the computation of the ATD collective mass and the zero-point vibrational energy correction ΔE_{vib} within the perturbative cranking approximation [16, 72–75]. Moreover, in this work we have also considered the alternative GCM-like (perturbative) collective masses and vibrational energy corrections [16]. Though the expression for these quantities lack a theoretical justification, as the one available in the ATD case, we have considered the GCM-like collective masses and vibrational energy corrections mostly to compare with the corresponding results already obtained for even-even U and Pu nuclei [13, 14].

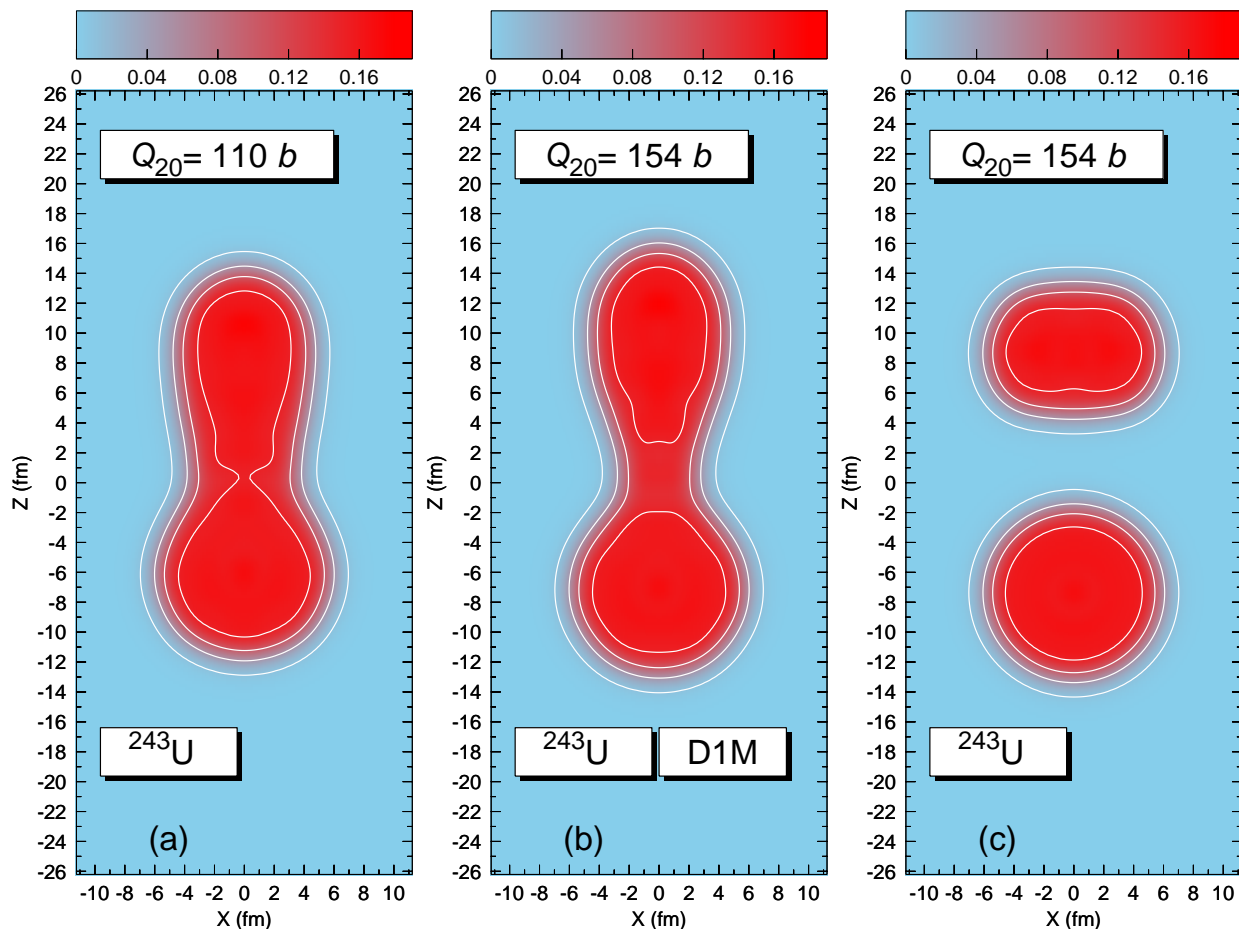


FIG. 2: (Color online) Density contour plots for the nucleus ^{243}U at the quadrupole deformations $Q_{20}=110$ b [panel (a)] and $Q_{20}=154$ b [panels (b) and (c)]. The density profiles in panels (a) and (b) correspond to 1F configurations while the one in panel (c) represents a 2F solution. Densities are in units of fm^{-3} and contour lines are drawn at 0.01, 0.05, 0.10 and 0.15 fm^{-3} . For more details, see the main text.

We have obtained the spontaneous fission half-life t_{SF} (in seconds) within the Wentzel-Krammers-Brillouin (WKB) formalism [76, 77]

$$t_{SF} = 2.86 \times 10^{-21} \times (1 + e^{2S}) \quad (3)$$

where the action S along the fission K_0 -path reads

$$S = \int_a^b dQ_{20} \sqrt{2B(Q_{20}) [V(Q_{20}) - (E_{Min} + E_0)]} \quad (4)$$

In this work, the path to fission is determined by using the least energy principle. This is a simplification over the alternative approach of considering the least action path. In Eq. (4), the integration limits a and b are the classical turning points for $E_{Min} + E_0$. The energy E_{Min} corresponds to the absolute minimum of the considered 1F K_0 -path while E_0 accounts for the true ground state energy once quadrupole fluctuations are considered. The value of E_0 could be estimated using the curvature

around the absolute minimum of the K_0 -path and the values of the collective inertias [15, 34]. However, we have followed the usual recipe [9, 13] and considered E_0 as a free parameter that takes four values (i.e., $E_0 = 0.5, 1.0, 1.5$ and 2.0 MeV). This allows us to estimate its impact on the predicted t_{SF} values [13–17]. On the other hand, the collective potential $V(Q_{20})$ is given by the HFB-EFA energy corrected by the zero-point rotational $\Delta E_{ROT}(Q_{20})$ and vibrational $\Delta E_{vib}(Q_{20})$ energies. We have overlooked the E_0 -dependence of the prefactor in front of the exponential Eq. (3) due to the large uncertainties in the estimation of the t_{SF} values arising from other sources. Furthermore, in the computation of the t_{SF} values Eq. (3), the wiggles in the collective masses have been softened by means of a three point filter [13].

Finally, in order to study the competition between the spontaneous fission and α -decay modes, we have computed the t_α lifetimes using the Viola-Seaborg formula [11]

$$\log_{10} t_\alpha = \frac{AZ + B}{\sqrt{Q_\alpha}} + CZ + D + h_{log} \quad (5)$$

with parameters given in [12]. The Q_α values (in MeV) are obtained from the calculated binding energies for U, Pu and Th nuclei. Within this context, the use of the Gogny-D1M EDF is particularly relevant as it provides a better description of the nuclear masses and it is expected to perform well in neutron-rich nuclei [57].

III. DISCUSSION OF THE RESULTS

In this section, we discuss the results of our calculations for odd-mass U and Pu nuclei. First, in Sec. III A we illustrate our methodology in the case of ^{243}U . The systematic of the fission paths, spontaneous fission half-lives as well as fragment mass and charge is presented in Sec. III B. In Sec. III C, we discuss the impact of pairing correlations on the predicted spontaneous fission half-lives. To this end, we have considered the Gogny-D1M EDF but with the strengths of the pairing fields increased by 5 and 10 %, respectively. For the sake of completeness, we also include in the corresponding figures results already obtained for even-even U and Pu nuclei [13, 14].

A. An illustrative example: The nucleus ^{243}U

In our calculations, ^{243}U is predicted to have a $K_0 = 9/2$ ground state with parity $\pi = -1$ (i.e., a $K_0^\pi = 9/2^-$ configuration). The 1F and 2F $K_0 = 9/2$ HFB-EFA plus the zero-point rotational energies, are plotted in panel (a) of Fig. 1 as functions of the quadrupole moment Q_{20} . We are dropping the parity of the ground state one-quasiparticle configuration to label the path to fission because in this specific example, parity is broken at large quadrupole deformations, beyond but near the fission isomer configuration. The zero-point vibrational energies ΔE_{vib} have not been included in the plot as they are rather constant as functions of the quadrupole moment. However, we always consider such vibrational corrections in the computation of the t_{SF} and t_α lifetimes as well as other relevant quantities such as barrier heights, excitation energies of fission isomers, etc. The octupole Q_{30} and hexadecapole Q_{40} moments are plotted in panel (b). In our calculations, an explicit constraint has not been included for \hat{Q}_{40} neither for other higher multipolarity operators. However, their average values are automatically adjusted during the selfconsistent minimization of the HFB-EFA energy.

As can be seen from the figure, the absolute minimum of the $K_0 = 9/2$ 1F path appears at $Q_{20} = 14\text{b}$. The first $9/2^-$ fission isomer at $Q_{20} = 44\text{b}$ lies 4.28 MeV above the ground state from which, it is separated by the inner barrier ($Q_{20} = 28\text{b}$) with the height of 10.05 MeV. Another noticeable feature from panel (a) is, the presence of a second octupole deformed fission isomer at $Q_{20} = 88\text{b}$ that lies 5.91 MeV above the ground state. As we will see later on (see, Sec. III B), second fission isomers are obtained for other odd-mass U and Pu nuclei. Those

minima have already been found in previous Gogny-D1M calculations for even-even systems along both isotopic chains [13, 14] as well as for other nuclei in this region of the nuclear chart [15]. This indicates that the shell effects [17, 28, 78–84] leading to those second fission isomers are systematically present in our mean-field calculations. A second barrier with the height of 11.22 MeV is found at $Q_{20} = 64\text{b}$. As can be seen from panel (b), both the second barrier and the second fission isomer belong to the parity-breaking (i.e., $Q_{30} \neq 0$) sector of the $K_0 = 9/2$ 1F path in ^{243}U . In fact, the left-right symmetry of the path is broken for $Q_{20} \geq 54\text{b}$. An outer barrier, with the height of 8.40 MeV, is also visible at $Q_{20} = 112\text{b}$.

The previous values have been obtained with the $K_0 = 9/2$ configuration corresponding to the lowest energy for each quadrupole deformation (keep in mind that we assume the conservation of the K quantum number in the fission process). Therefore, they might or might not correspond to the lowest energy for a given Q_{20} . For example, at the location of the first fission isomer ($Q_{20} = 44\text{b}$) the configuration with the lowest energy corresponds to $K = 5/2$. On the other hand, at the location of the second fission isomer ($Q_{20} = 88\text{b}$) the configuration with the lowest energy corresponds to $K = 1/2$.

In each panel of Fig. 1, we have also included results corresponding to AV HFB calculations for ^{243}U . As can be seen from panel (a), the 1F and 2F HFB-EFA paths are always higher in energy than the AV ones. Moreover, the energy difference between the $K_0 = 9/2$ and AV paths is not constant as a function of Q_{20} . This is a manifestation of the specialization energy effect partly due to the fact that we are following configurations with a fixed $K_0 = 9/2$ quantum number. For example, the HFB-EFA inner, second and third barriers (10.05, 11.22 and 8.40 MeV) are higher than the AV ones (9.68, 10.72 and 8.05 MeV). The same is also true for the excitation energies of the HFB-EFA first and second fission isomers (4.28 and 5.91 MeV) when compared with the AV ones (4.02 and 5.82 MeV).

As can be seen from panels (a) and (b), not only the quadrupole but also the octupole and hexadecapole moments of the HFB-EFA and AV paths exhibit a rather similar behavior. This shows the very minute impact of blocking in the mass moments characterizing the shape of ^{243}U . Panel (b) also reveals that the Q_{30} and Q_{40} moments corresponding to the 1F [i.e., $Q_{30}(1F)$ and $Q_{40}(1F)$] and 2F [i.e., $Q_{30}(2F)$ and $Q_{40}(2F)$] paths are rather different due to their separation in the multidimensional space of deformations.

In the case of ^{243}U , as a result of projecting multidimensional fission $K_0 = 9/2$ paths into the one-dimensional plot of the figure, the HFB-EFA 1F and 2F curves appear as intersecting ones. However, in the multidimensional space of deformation parameters, there is a $9/2$ -path with a ridge connecting them. For ^{243}U as well as for all the other odd-mass nuclei studied in this work, we have neglected the contribution of such a path [13–15] to the collective action Eq. (4). This amounts to take

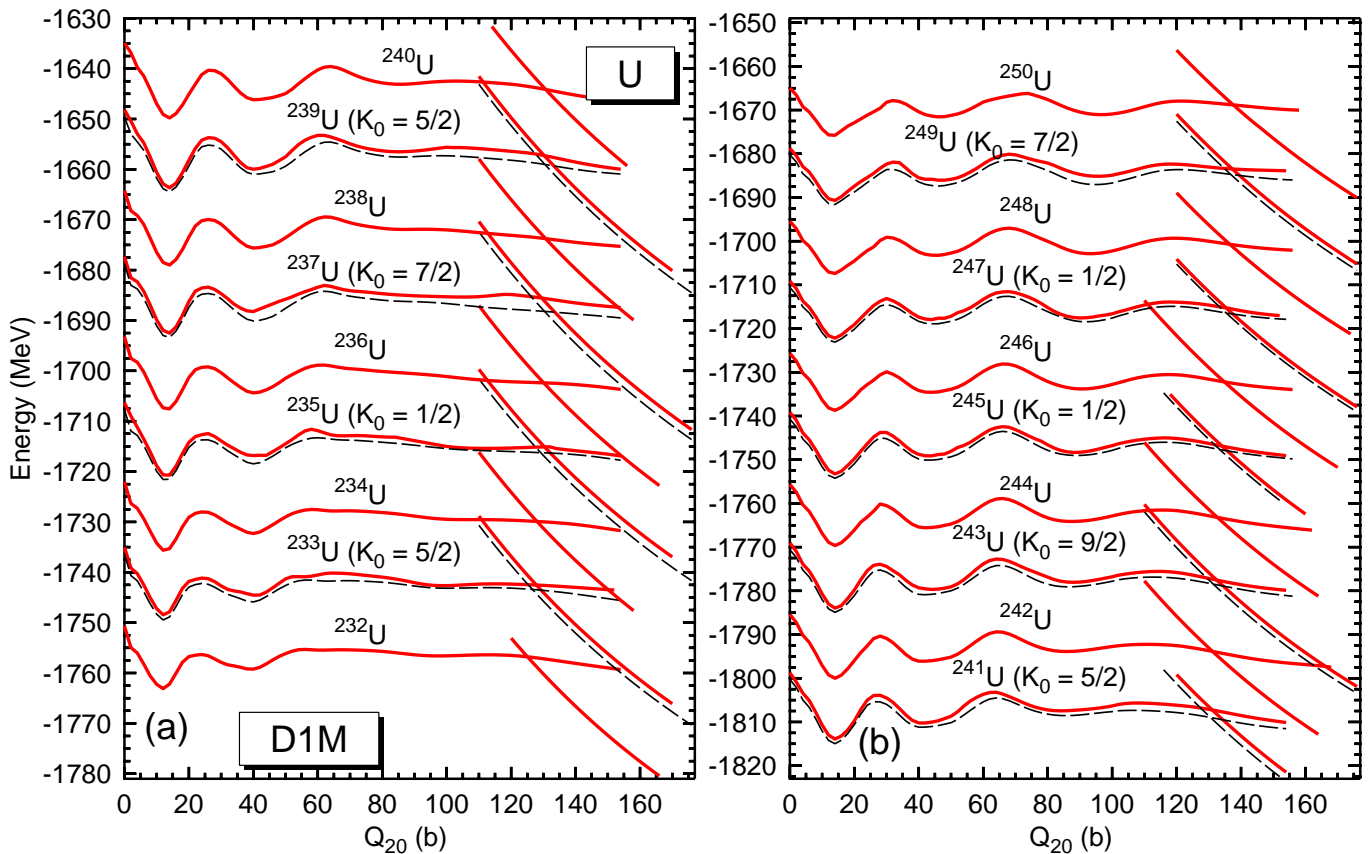


FIG. 3: (Color online) The ground state fission paths obtained for odd-mass U isotopes are plotted as functions of the quadrupole moment Q_{20} . The fission paths for even-even isotopes are taken from Ref. [13]. Starting from the nucleus ^{233}U (^{242}U) in panel (a) [panel (b)], the curves have been shifted by 20 MeV in order to accommodate them in a single plot. For odd-mass nuclei, the corresponding K_0 values are included in the plot. The "average" (AV) fission paths for those odd-mass U nuclei are also depicted with dashed lines. For more details, see the main text.

the HFB-EFA 1F and 2F curves as really intersecting in the computation of the spontaneous fission half-life.

In panel (c) of Fig. 1, we have plotted the HFB-EFA and AV pairing energies. On the one hand, the proton pairing energies can hardly be distinguished. On the other hand the HFB-EFA and AV neutron pairing energies display a similar trend with pronounced minima (maxima) around the Q_{20} values corresponding to the ground state, the first and second fission isomers (the top of the inner and second barriers). Nevertheless, the HFB-EFA neutron pairing energies tend to be smaller than the AV ones as a result of the quenching of pairing correlations via blocking. As a consequence of this quenching, there is an enhancement of the ATD and/or GCM masses with respect to the AV ones, as can be seen from panels (d) and (e), respectively. We then conclude that the unpaired neutron leads to both the specialization energy effect and to the increase of the collective masses regardless of the ATD and/or GCM scheme employed in their computation. Both effects go in the direction of increasing the collective action and, in turn, to larger spontaneous fission half-lives in odd-mass U and Pu nuclei as compared with their even-even neighbors

(see, Sec. III B).

Furthermore, the ATD masses are larger than the GCM ones [13–16]. In fact, such a difference is the reason why we have considered both kinds of collective masses in the computation of the spontaneous fission half-lives even, when there is a lack of theoretical justification for the use of the latter in the case of odd-mass nuclei. For example, in the case of ^{243}U and $E_0 = 1.0$ MeV, the ATD masses lead to $\log_{10} t_{SF} = 60.5530$ s while the GCM ones lead to $\log_{10} t_{SF} = 39.2109$ s. On the other hand, increasing the value of E_0 provides a reduction in the t_{SF} values. For example, for $E_0 = 1.5$ MeV, we have obtained $\log_{10} t_{SF} = 56.5407$ s and $\log_{10} t_{SF} = 36.5494$ s within the ATD and GCM schemes, respectively.

The density contour plots corresponding to the nucleus ^{243}U at the quadrupole deformations $Q_{20} = 110$ and 154 b are shown in panels (a), (b) and (c) of Fig. 2. For $Q_{20} = 154$ b, two plots are shown corresponding to 1F and 2F solutions, respectively. The 2F solution in panel (c), corresponds to a spherical ^{132}Sn fragment plus an oblate ($\beta_2 = -0.21$) and slightly octupole deformed ($\beta_3 = 0.02$) ^{111}Mo fragment. The shape of ^{111}Mo minimizes a Coulomb repulsion energy of 186.50 MeV. Oblate de-

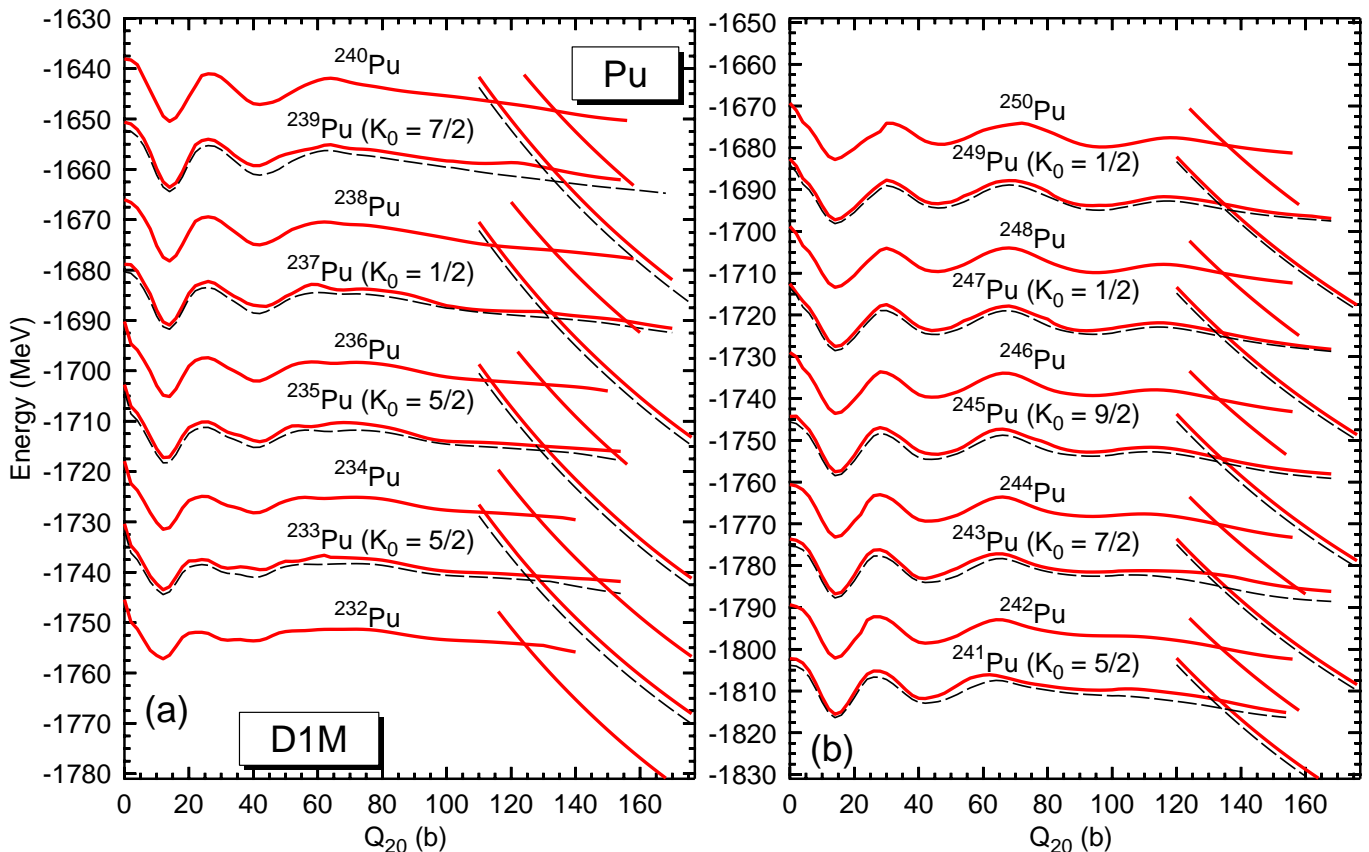


FIG. 4: (Color online) The ground state fission paths obtained for odd-mass Pu isotopes are plotted as functions of the quadrupole moment Q_{20} . The fission paths for even-even isotopes are taken from Ref. [14]. Starting from the nucleus ^{233}Pu (^{242}Pu) in panel (a) [panel (b)], the curves have been shifted by 20 MeV in order to accommodate them in a single plot. For odd-mass nuclei, the corresponding K_0 values are included in the plot. The "average" (AV) fission paths for those odd-mass Pu nuclei are also depicted with dashed lines. For more details, see the main text.

formed fragments have been obtained in previous studies [13–15, 17] as well as by fissioning other odd-mass U and Pu nuclei as we will see later on in this paper (see, Sec. III B). The previous results, illustrate the key role played by the shell effects associated with the proton $Z=50$ and neutron $N=82$ magic numbers [85–87] in determining the charge and mass of the fission fragments. On the one hand, this could be expected within the framework of Ritz-variational approaches [13–15] and, in particular, the HFB-EFA. On the other hand, the available data [88, 89] indicate that, for the considered region, the heavy fragment mass number is close to $A=140$ instead of $A=132$. In our calculations the properties of the fragments are determined by 2F solutions of the HFB-EFA equations at the largest Q_{20} values (see, Fig. 1). Nevertheless, such 2F solutions are not necessarily the ones corresponding to scission products. A more realistic approximation to the mass and charge of the fission fragments has to include dynamical effects around the loosely defined scission configuration [90, 91]. Moreover, our calculations do not account for the broad mass distribution observed experimentally. Therefore, the values obtained should be taken only as an approximation to

the peaks in that distribution.

B. Systematic of the fission paths, spontaneous fission half-lives and fragment mass and charge in odd-mass U and Pu nuclei

In Fig. 3, we have summarized the ground state fission paths obtained for the nuclei $^{233,235,237,239}\text{U}$ [panel (a)] and $^{241,243,245,247,249}\text{U}$ [panel (b)]. The fission paths for the isotopes $^{233,235,237,239}\text{Pu}$ and $^{241,243,245,247,249}\text{Pu}$ are shown in panels (a) and (b) of Fig. 4. The corresponding K_0 values are also given in the plots. The AV fission paths obtained for those odd-mass nuclei are depicted with dashed lines. Results for even-even U and Pu nuclei are taken from Refs. [13] and [14]. The fission paths for odd-mass U and Pu nuclei exhibit a structural evolution similar to the one obtained for the corresponding even-even counterparts. The ground state is located around $Q_{20} = 14$ b while first fission isomers are found in the range of quadrupole moments $36 \leq Q_{20} \leq 44$ b. Those first isomers are separated from the ground state by the corresponding inner barriers the tops of which correspond

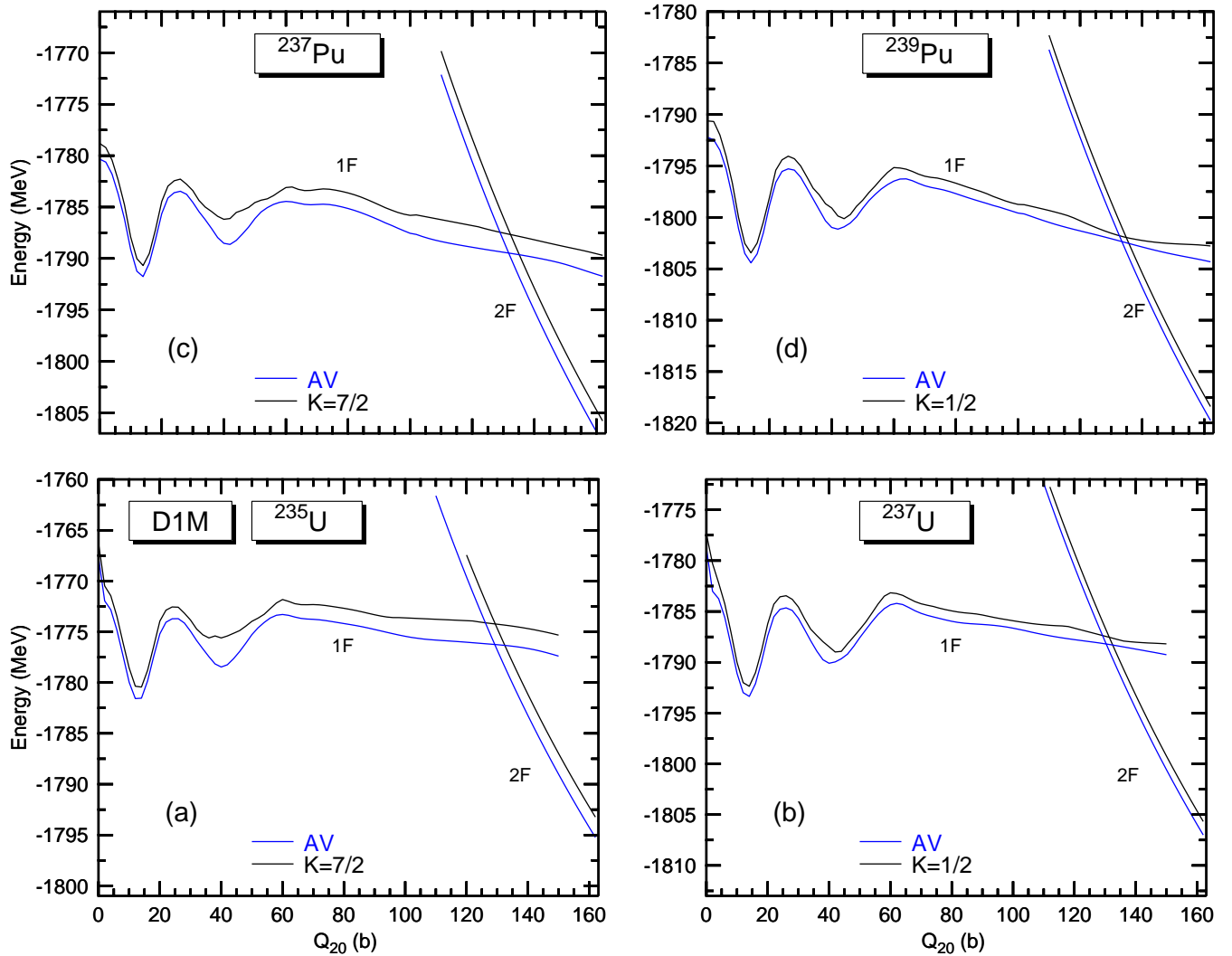


FIG. 5: (Color online) The $K = 7/2$ and $1/2$ HFB-EFA plus the zero point rotational energies, are plotted in panels (a) [(c)] and (b) [(d)] for the nuclei ^{235}U and ^{237}U (^{237}Pu and ^{239}Pu) as functions of the quadrupole moment Q_{20} . Both the 1F and 2F solutions are included in the plots. Results corresponding to "average" (AV) HFB calculations for ^{235}U , ^{237}U , ^{237}Pu and ^{239}Pu have also been included in the panels. For more details, see the main text.

to $22 \leq Q_{20} \leq 30$ b. The heights of those inner barriers can be reduced, by a few MeV, due to triaxiality [13]. Moreover, in the case of odd-mass nuclei the polarization effects associated with the unpaired nucleon might also lead to triaxial solutions. In our calculations, we have kept axial symmetry as a self-consistent symmetry along the whole fission path in order to reduce the computational effort. On the other hand, the already mentioned lowering of the inner barriers, by the γ degree of freedom, comes together with an increase of the collective inertia [7, 35] that tends to compensate in the final value of the action Eq. (4). Therefore, the role of the γ deformation parameter in the spontaneous fission half-lives is very limited [35]. On the other hand, the tops of the second barriers correspond to $52 \leq Q_{20} \leq 70$ b.

From the figures, one also realizes that second fission isomers appear for several even-even and odd-mass U and

Pu nuclei indicating that the corresponding shell effects are systematically present in our Gogny-D1M calculations for this region of the nuclear chart [13–15]. Those parity-breaking second isomers become apparent around ^{239}U and ^{243}Pu and their quadrupole moments lie within the range $84 \leq Q_{20} \leq 96$ b. With increasing neutron number, outer barriers also emerge along the 1F paths with their tops corresponding to quadrupole deformations $Q_{20} \geq 110$ b. Furthermore, the comparison between the HFB-EFA ground state and AV (1F and 2F) paths reveals the specialization energy effects in the case of odd-mass systems.

From the experimental point of view the ground states of the nuclei $^{233,235,237,239}\text{U}$ correspond to $5/2^+$, $7/2^-$, $1/2^+$ and $5/2^+$ configurations, respectively. On the other hand, the nuclei $^{235,237,239,241,243,245,247}\text{Pu}$ have $5/2^+$, $7/2^-$, $1/2^+$, $5/2^+$, $7/2^+$, $9/2^-$ and $1/2^+$ ground states

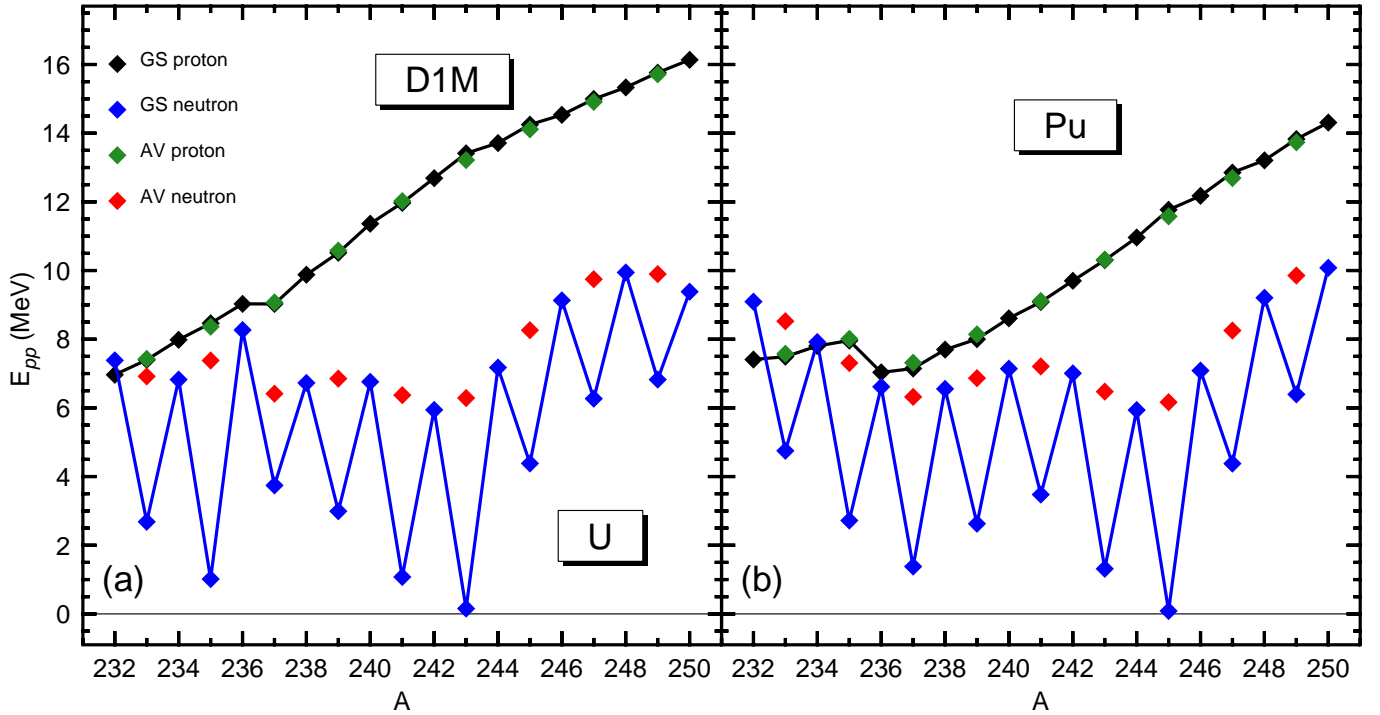


FIG. 6: (Color online) The proton and neutron pairing interaction energies E_{pp} corresponding to the ground states (GS) of $^{232-250}\text{U}$ [panel (a)] and $^{232-250}\text{Pu}$ [panel (b)] are plotted as functions of the mass number A . Results for even-even U and Pu nuclei are taken from Refs. [13] and [14]. The "average" (AV) E_{pp} values obtained for odd-mass nuclei are also included in the plots.

[92]. Our calculations, agree well with the available data for $^{233,239}\text{U}$ and $^{235,241,243,245,247}\text{Pu}$. On the other hand, given the discrepancy between our predictions and the experimental K_0 values, in the case of ^{235}U and ^{237}U (^{237}Pu and ^{239}Pu) we have also explored the $K = 7/2$ and $1/2$ paths. They are plotted in Fig. 5 as functions of the quadrupole moment Q_{20} . Both their structure and the corresponding specialization energy effects are similar to the ones for the ground state fission paths in Figs. 3 and 4.

The proton and neutron ground state (GS) pairing interaction energies E_{pp} [25] are plotted in panels (a) and (b) of Fig. 6 as functions of the mass number A . The AV E_{pp} values obtained for odd-mass nuclei are also included in the plots. The HFB-EFA and AV proton pairing energies are rather similar and exhibit a sharp increase with increasing mass number A . On the other hand, the quenching of the HFB-EFA neutron pairing with respect to the AV one, via blocking, is rather pronounced. As a measure of how effective is the quenching of the neutron pairing correlations in the ground states of the odd-mass systems, one can take the ratio $r = \langle \Delta \hat{N}^2 \rangle_{GS} / \langle \Delta \hat{N}^2 \rangle_{AV}$ [16]. We have obtained the values $r = 0.360, 0.367, 0.579, 0.667, 0.631, 0.103, 0.661, 0.839$ and 0.814 for the U isotopes with $A = 233, \dots, 249$ while for the Pu isotopes with the same mass numbers the corresponding values are $r = 0.817, 0.457, 0.380, 0.631, 0.717, 0.332, 0.07, 0.653$ and 0.843 . For the absolute minima of the $K = 7/2$ and

$1/2$ paths (Fig. 5) in ^{235}U and ^{237}U (^{237}Pu and ^{239}Pu) we have obtained the ratios $r = 0.70$ and 0.78 (0.65 and 0.77). From the previous results we conclude that, at least for some of the studied odd-mass U and/or Pu nuclei, a more realistic treatment of pairing (including the role of dynamical fluctuations and their coupling to the relevant deformation parameters [26]) is required to describe the fission process. Work along these lines is in progress and will be reported elsewhere.

The inner barrier heights B_I [panels (a) and (b)], excitation energies of the first fission isomers E_I [panels (c) and (d)] and the second barrier heights B_{II} [panels (e) and (f)] are depicted in Fig. 7. The AV B_I , E_I and B_{II} values obtained for odd-mass nuclei are also included in the plots. With few exceptions, the HFB-EFA values exhibit odd-even as well as the specialization energy effects already discussed in the case of ^{243}U (Sec. III A). Similar trends are obtained for the excitation energies of the second fission isomers and the heights of the outer barriers in the case of heavier nuclei. Note that, as already discussed above, the heights of the inner barriers might be reduced, by a few MeV, due to triaxiality [13]. In our calculations the largest B_I , E_I and B_{II} values of 10.07 (10.56), 4.65 (4.31) and 11.22 (10.19) MeV are obtained for ^{241}U (^{243}Pu), ^{249}U (^{239}Pu) and ^{243}U (^{245}Pu), respectively. Furthermore, we have obtained the B_I , E_I and B_{II} values of 7.88, 4.84 and 8.62 MeV (8.40, 4.49 and 7.64 MeV) for the $K = 7/2$ path in ^{235}U (^{237}Pu) while

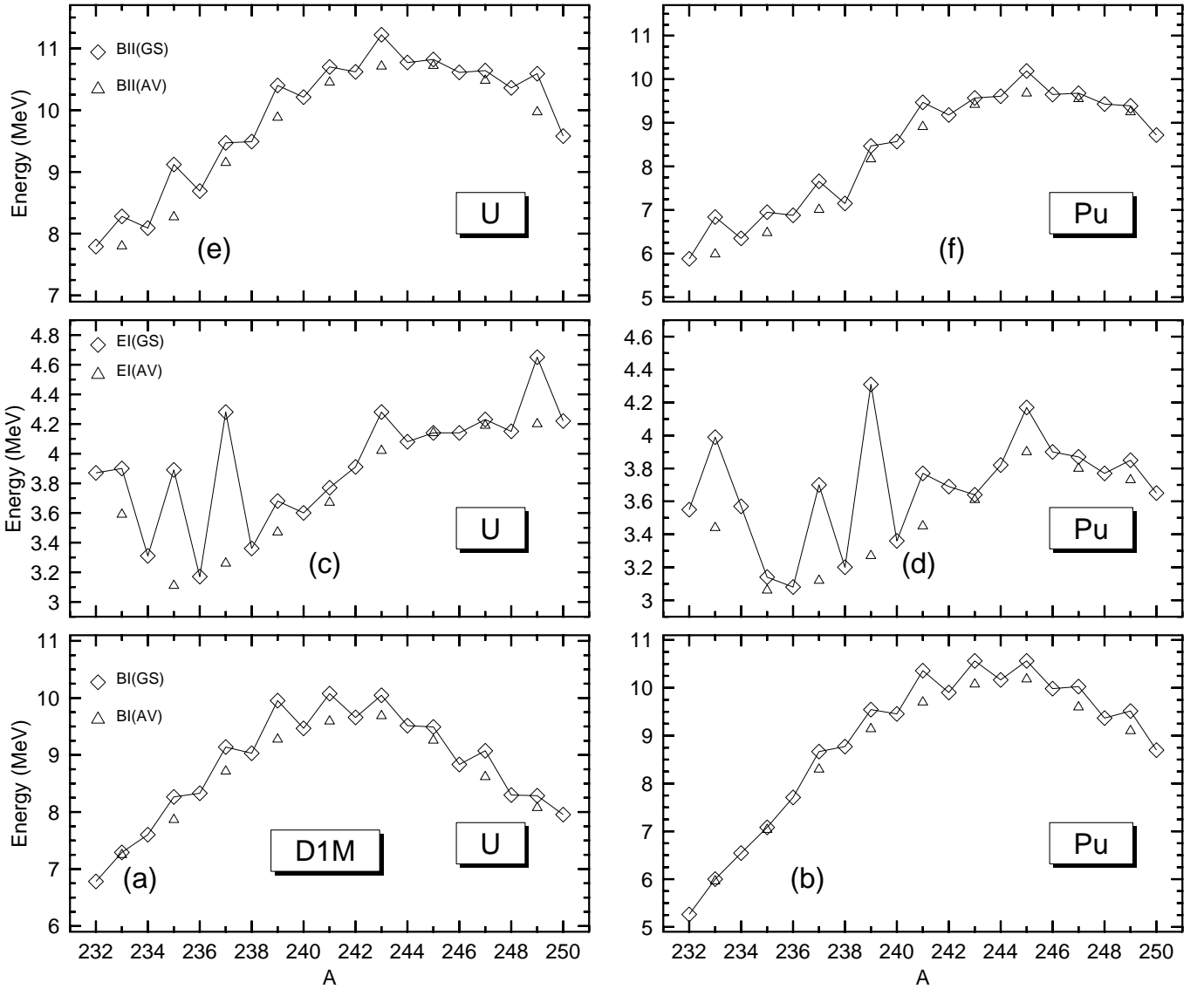


FIG. 7: The inner barrier height B_I [panels (a) and (b)], excitation energy of the first fission isomer E_I [panels (c) and (d)] and the second barrier height B_{II} [panels (e) and (f)] corresponding to the ground-state (GS) fission paths in odd mass U and Pu isotopes with $A=233, \dots, 249$ are plotted as functions of the mass number A . Results for even-even U and Pu nuclei are taken from Refs. [13] and [14]. The "average" (AV) B_I , E_I and B_{II} values obtained for odd-mass U and Pu nuclei are also included in the plot.

the corresponding values for the $K = 1/2$ path in ^{237}U (^{239}Pu) are 8.91, 3.38 and 9.20 MeV (9.40, 3.32 and 8.29 MeV). These values, should be compared with the ones shown in the figure, i.e., 8.27, 3.89 and 9.12 MeV (8.66, 3.70 and 7.76 MeV) for the ground state fission path of ^{235}U (^{237}Pu) and 9.14, 4.28 and 9.47 MeV (9.54, 4.31 and 8.47 MeV) for the ground state path of ^{237}U (^{239}Pu).

For all the studied odd-mass nuclei, we have also obtained a pronounced enhancement of the ATD and/or GCM collective masses, with respect to the AV ones, which results from the quenching of the neutron pairing correlations by the unpaired neutron (see, Figs. 1 and 6). Both the specialization energy effects described

above and the enhancement of the collective masses, are the main factors leading, as we will see later on, to larger spontaneous fission half-lives in the odd mass U and Pu isotopes considered, as compared with their even-even neighbors [16].

In Fig. 8, we have depicted the spontaneous fission half-lives, predicted within the GCM and ATD schemes, for U [panel (a)] and Pu [panel (b)] nuclei as functions of the mass number A . For each nucleus, calculations have been carried out with $E_0 = 0.5, 1.0, 1.5$ and 2.0 MeV. The experimental values shown in the figure for ^{232}U and ^{233}U correspond to lower bounds. No experimental t_{SF} value is available for ^{237}U [53]. In the case

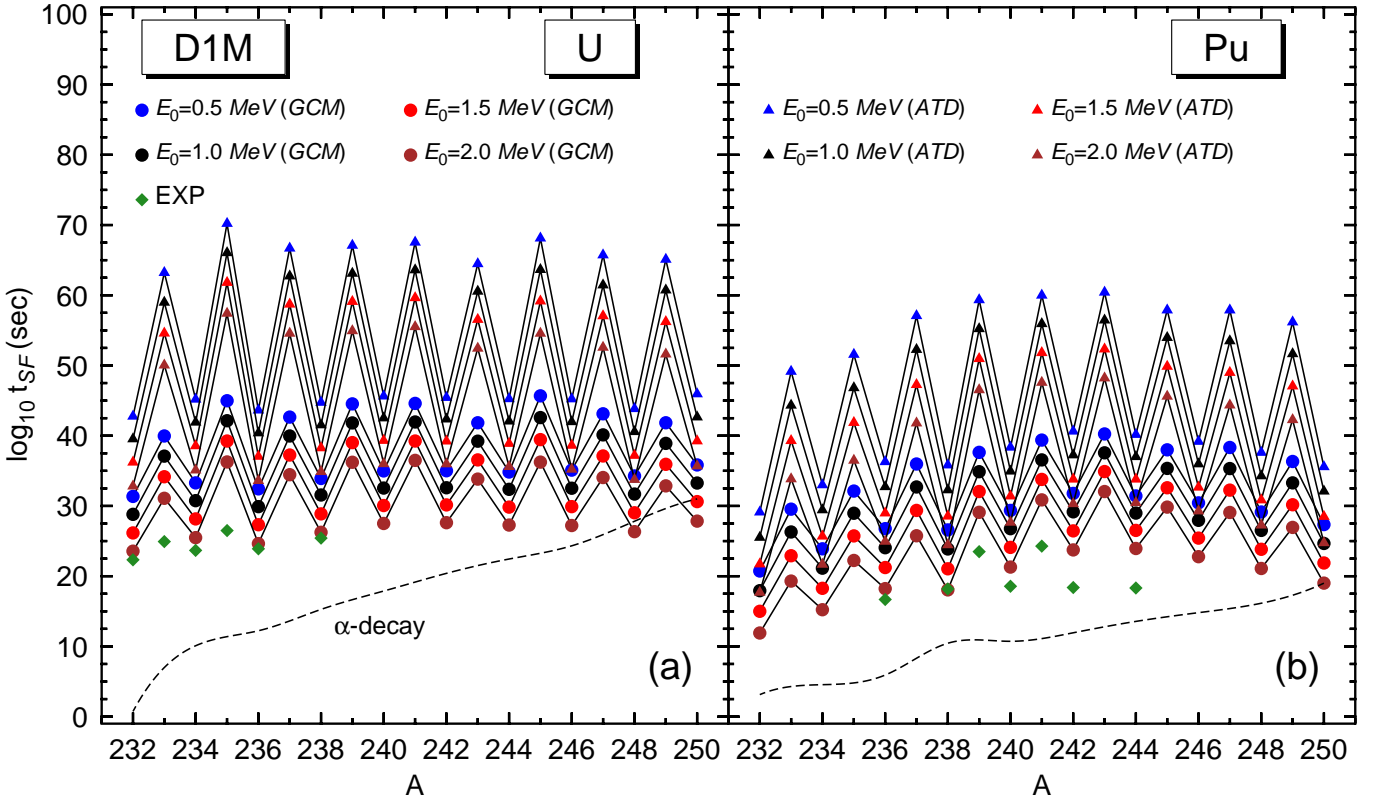


FIG. 8: (Color online) The spontaneous fission half-lives, predicted within the GCM and ATD schemes, for the nuclei $^{232-250}\text{U}$ [panel (a)] and $^{232-250}\text{Pu}$ [panel (b)] are depicted as functions of the mass number A . For each nucleus, calculations have been carried out with $E_0 = 0.5, 1.0, 1.5$ and 2.0 MeV. Results for even-even U and Pu nuclei are taken from Refs. [13] and [14]. The experimental t_{SF} values are taken from Ref. [53]. In addition, α -decay half-lives are plotted with short dashed lines. For more details, see the main text.

TABLE I: The values of $\log_{10} t_{SF}$ (in s) obtained for the $K = 7/2$ path in ^{235}U (^{237}Pu) and the $K = 1/2$ path in ^{237}U (^{239}Pu) are given as functions of the parameter E_0 (in MeV). For details, see the main text.

Nucleus	K	Scheme	$E_0=0.5$ MeV	$E_0 = 1.0$ MeV	$E_0 = 1.5$ MeV	$E_0 = 2.0$ MeV
^{235}U	7/2	GCM	40.2335	37.4653	34.6713	31.7890
^{235}U	7/2	ATD	65.6648	61.5757	57.4544	53.2159
^{237}U	1/2	GCM	44.2782	41.2471	38.1644	34.9754
^{237}U	1/2	ATD	68.1143	63.7326	59.2679	54.6358
^{237}Pu	7/2	GCM	34.3406	31.4090	28.3981	25.2630
^{237}Pu	7/2	ATD	56.4852	52.1555	47.7064	43.0442
^{239}Pu	1/2	GCM	36.2572	33.0818	29.7459	26.1170
^{239}Pu	1/2	ATD	57.2207	52.5042	47.4956	42.0561

of ^{241}Pu the value shown in the figure corresponds to an upper bound while no experimental data are available for $^{232,233,234,235,237,243}\text{Pu}$ [53]. The data reveal an increase in the spontaneous fission half-lives of the odd-mass nuclei as compared with their even-even neighbors. Such a

trend is also observed in our calculations. Increasing the parameter E_0 leads to a decrease in the predicted t_{SF} values as well as to an improvement of the agreement with the experiment. That larger E_0 values are required for a better comparison with the experiment is, a con-

sequence of the fact that the Gogny-D1M EDF provides wide 1F curves with a gentle decline [13]. In Sec. III C, we will also discuss the impact of pairing correlations on the predicted t_{SF} values.

The ATD spontaneous fission half-lives are larger than the GCM ones, with the difference being more pronounced for odd-mass nuclei. For example, for ^{247}U and ^{247}Pu with $E_0 = 1.0$ MeV we have obtained $\log_{10} t_{SF} = 61.4421$ s and $\log_{10} t_{SF} = 53.5035$ s within the ATD scheme while the corresponding GCM values are $\log_{10} t_{SF} = 40.1248$ s and $\log_{10} t_{SF} = 35.3381$ s, respectively (see also, table I). The previous results already reveal the strong variance of the predicted t_{SF} values with respect to the details involved in their computation (see also, Sec. III C). However, regardless of the scheme and/or E_0 value employed, the same trend emerges from our calculations, i.e., the fission lifetimes exhibit a pronounced odd-even staggering. For a given odd-mass nucleus, the amplitude of the staggering can be defined as

$$\delta_{st} = \log_{10} t_{SF}(\text{odd}) - \log_{10} t_{SF}(\text{ee}, \text{av}) \quad (6)$$

where $t_{SF}(\text{odd})$ represents its spontaneous fission half-life while $t_{SF}(\text{ee}, \text{av})$ is the average value for the two even-even neighbors. We have studied such a quantity and found that it depends strongly on both the neutron number and the type of collective mass employed, with the ATD values δ_{st}^{ATD} being larger than the GCM δ_{st}^{GCM} ones. For example for the nuclei ^{233}U (^{233}Pu) and ^{241}U (^{241}Pu) we have obtained, with $E_0 = 1.0$ MeV, the ATD values $\delta_{st}^{ATD} = 17.3711$ s (15.2123 s) and $\delta_{st}^{ATD} = 21.1714$ s (18.9971 s) while the GCM staggering for those nuclei are $\delta_{st}^{GCM} = 6.6337$ s (5.4624 s) and 9.3843 s (7.6828 s), respectively. On the other hand, the amplitude of the staggering is rather insensitive to E_0 . Note, that similar features to the ones already mentioned emerge if we consider (see table I) the $K = 7/2$ path in ^{235}U (^{237}Pu) and the $K = 1/2$ path in ^{237}U (^{239}Pu).

In addition, in Fig. 8 we have plotted the α -decay half-lives computed with a parametrization [12] of the Viola-Seaborg formula [11]. We have used the binding energies obtained for U, Pu and Th nuclei. We conclude that, though α -decay is the dominant decay channel for most of the studied nuclei, the steady increase in the t_α values as functions of the mass number A, leads to a pronounced competition with spontaneous fission around $A = 248$ -250. This agrees well with previous fission calculations for Ra [15], U [13] and Pu [14] nuclei which suggest that as we move to the very neutron-rich sectors of the corresponding isotopic chains, fission turns out to be faster than α -decay.

The proton (Z_1, Z_2), neutron (N_1, N_2) and mass (A_1, A_2) numbers of the fission fragments are plotted, as functions of the mass number A in the parent nucleus, in Fig. 9. The key role played by the proton $Z=50$ and neutron $N=82$ magic numbers in the masses and charges of the predicted fission fragments is apparent from the figure. However, the properties of those fragments are determined by Ritz-variational solutions of the HFB-EFA

equations along the 2F curves (see, Figs. 1, 3 and 4) at the largest quadrupole moments. Therefore, caution should be taken when comparing with available experimental data for this region of the nuclear chart (see, for example, [88, 89, 93]).

We have also studied the shapes of the fission fragments. As illustrative examples, we have plotted in Fig. 10 the density contour plots for ^{239}U [panel (a)], ^{239}Pu [panel (b)] and ^{249}Pu [panel (c)] at the quadrupole deformations $Q_{20}=150, 148$ and 150 b, respectively. For both ^{239}U and ^{249}Pu , a spherical ^{132}Sn heavier fragment is predicted while the lighter fragments correspond to oblate and slightly octupole deformed ^{107}Mo ($\beta_2 = -0.23, \beta_3 = 0.02$) and ^{117}Ru ($\beta_2 = -0.19, \beta_3 = 0.02$) nuclei, respectively. In the case of ^{239}Pu our calculations predict an almost spherical heavier fragment with $Z = 50.67$ and $N = 80.99$ while the deformed ($\beta_2 = -0.23, \beta_3 = 0.02$) lighter fragment has $Z = 43.33$ and $N = 64$. The predicted oblate fragments in ^{239}U , ^{239}Pu and ^{249}Pu minimize large Coulomb repulsion energies of 187.00, 196.79 and 200.66 MeV. The appearance of oblate fragments in our calculations for even-even [13, 14] and odd-mass U and Pu nuclei, as well as for other systems in this region of the nuclear chart [15], deserves further attention as fission fragments are usually assumed to have prolate shapes [94, 95].

C. Varying pairing strengths in odd-mass U and Pu nuclei

In this section, we discuss the impact of pairing correlations on the predicted spontaneous fission half-lives. We have carried out calculations, along the lines discussed in Sec. II, but with a modified Gogny-D1M EDF in which a factor η has been introduced in front of the pairing fields [25]. For simplicity, we have considered the same $\eta = 1.05$ and 1.10 factor for both protons and neutrons [13]. Let us mention, that the main reason to consider modified strengths is that, as we have seen in Secs. III A and III B, pairing correlations are key ingredients in the computation of the collective masses as well as the zero-point rotational and vibrational quantum corrections [13–15, 55, 56].

The $K_0 = 9/2$ HFB-EFA plus the zero point rotational energies obtained with the normal ($\eta=1.00$) and modified ($\eta=1.05$ and $\eta=1.10$) Gogny-D1M EDF are plotted in panel (a) of Fig. 11 as functions of the quadrupole moment Q_{20} for the nucleus ^{243}U , taken as an illustrative example. Similar calculations have been carried out for all the nuclei studied in this paper. For each η value, both the 1F and 2F solutions are included in the plot. The octupole Q_{30} and hexadecapole Q_{40} moments corresponding to the 1F and 2F solutions are shown in panel (b) of the figure. The 1F and 2F curves, for ^{243}U and all the studied odd-mass nuclei, exhibit rather similar shapes for different η -values. Note, however, that the energy shifts obtained for $\eta = 1.05$ and/or $\eta = 1.10$ depend

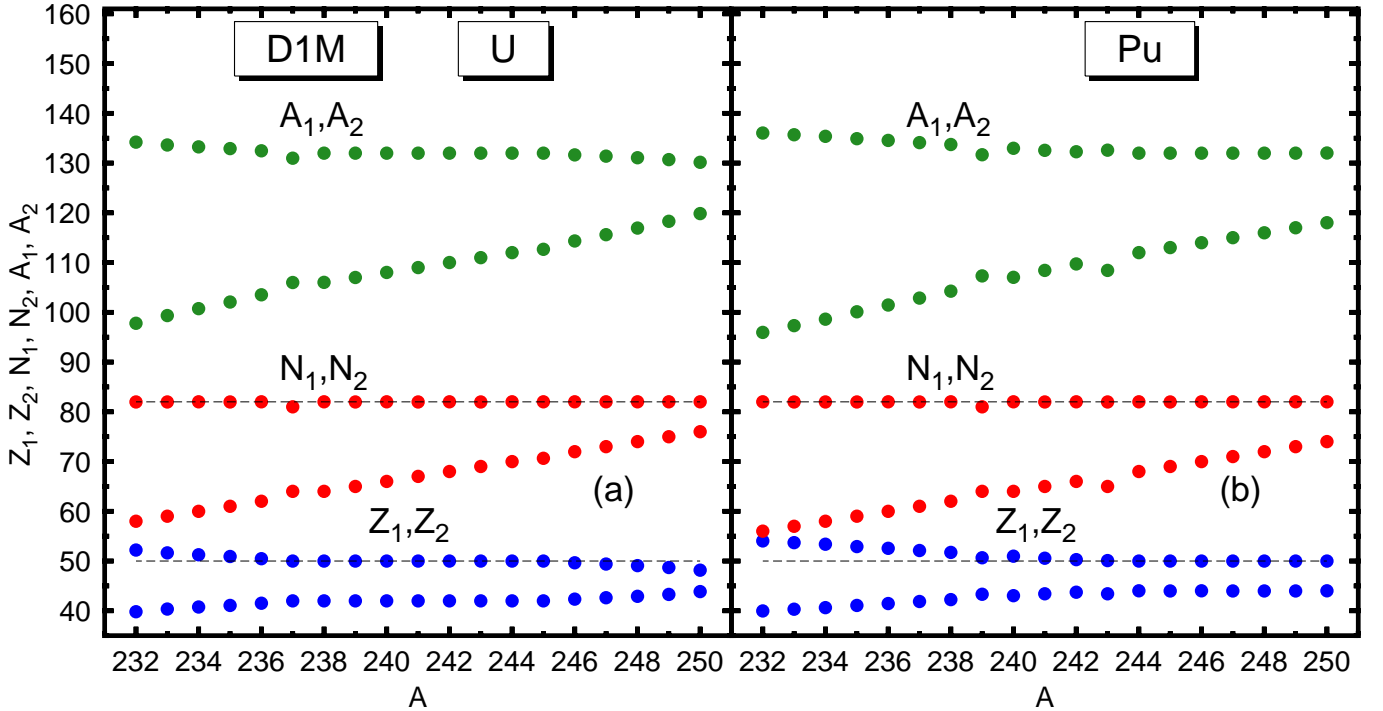


FIG. 9: (Color online) The proton (Z_1, Z_2), neutron (N_1, N_2) and mass (A_1, A_2) numbers of the two fragments resulting from the fission of $^{232-250}\text{U}$ [panel (a)] and $^{232-250}\text{Pu}$ [panel (b)] are shown as functions of the mass number A in the parent nucleus. Results for even-even U and Pu nuclei are taken from Refs. [13] and [14]. The magic proton $Z = 50$ and neutron $N = 82$ numbers are highlighted with dashed horizontal lines to guide the eye.

on the quadrupole moment. For example, in the case of ^{243}U , the energy gain for the $K_0^\pi = 9/2^-$ ground state is 1.23 (2.91) MeV while the heights of the inner and second barriers are reduced by 0.73 (1.55) and 0.46 (0.92) MeV for $\eta = 1.05$ ($\eta = 1.10$) when compared with the values obtained with the normal Gogny-D1M EDF. On the other hand, the octupole and hexadecapole moments of both the 1F and 2F solutions, can hardly be distinguished for different η -values. In panel (c) of the figure, we have depicted the pairing interaction energies for protons (dashed lines) and neutrons (full lines). We observe the same trend though the pairing energies increase with increasing η -values.

The collective ATD and GCM masses are plotted in panels (d) and (e) of Fig. 11. Regardless of the ATD and/or GCM scheme, we observe a reduction of the collective masses for increasing η -values. This agrees well with previous results [13–15, 17] as well as with the inverse dependence of the collective masses on the square of the pairing gap [55, 56]. Such a reduction has a strong impact on the predicted t_{SF} values. For example, in the case of ^{243}U and $E_0 = 1.0$ MeV, we have obtained $\log_{10} t_{SF} = 60.5530$ s, $\log_{10} t_{SF} = 54.9162$ s and $\log_{10} t_{SF} = 49.7725$ s within the ATD scheme for $\eta = 1.00, 1.05$ and 1.10 , respectively. The corresponding GCM values are $\log_{10} t_{SF} = 39.2109$ s, $\log_{10} t_{SF} = 31.4145$ s and $\log_{10} t_{SF} = 24.9485$ s.

In Fig. 12 we have plotted, the spontaneous fission half-

lives, predicted within the GCM and ATD schemes, for U isotopes as functions of the mass number A . The t_{SF} values obtained for Pu isotopes are shown in Fig. 13. Results have been obtained with the normal ($\eta = 1.00$) and modified ($\eta = 1.05$ and 1.10) Gogny-D1M EDF. Calculations have been carried out with $E_0 = 0.5$ [panel (a)], 1.0 [panel (b)], 1.5 [panel (c)] and 2.0 MeV [panel (d)], respectively. The experimental t_{SF} values are taken from Ref. [53]. In addition, α -decay half-lives are also included in the plots with short dashed lines.

As can be seen from Figs. 12 and 13, increasing the strengths of the pairing fields by 5 or 10 % leads to a pronounced reduction of several orders of magnitude in the predicted spontaneous fission half-lives. This is a consequence of the corresponding reduction in the ATD and/or GCM collective masses. Such a reduction in the predicted t_{SF} values also tends to improve the agreement with the available experimental data, especially within the GCM scheme. However, regardless of the η value, the predicted ATD spontaneous fission half-lives remain larger than the GCM ones. In the case of the odd-mass nuclei we have found, that the amplitude of the staggering does not exhibit a pronounced reduction as a function of η , with the ATD values being larger than the GCM ones. The amplitude of the staggering could be reduced in our calculation by considering that dynamical pairing correlations are expected to be larger for the odd isotopes than for the even ones. However, a qualitative

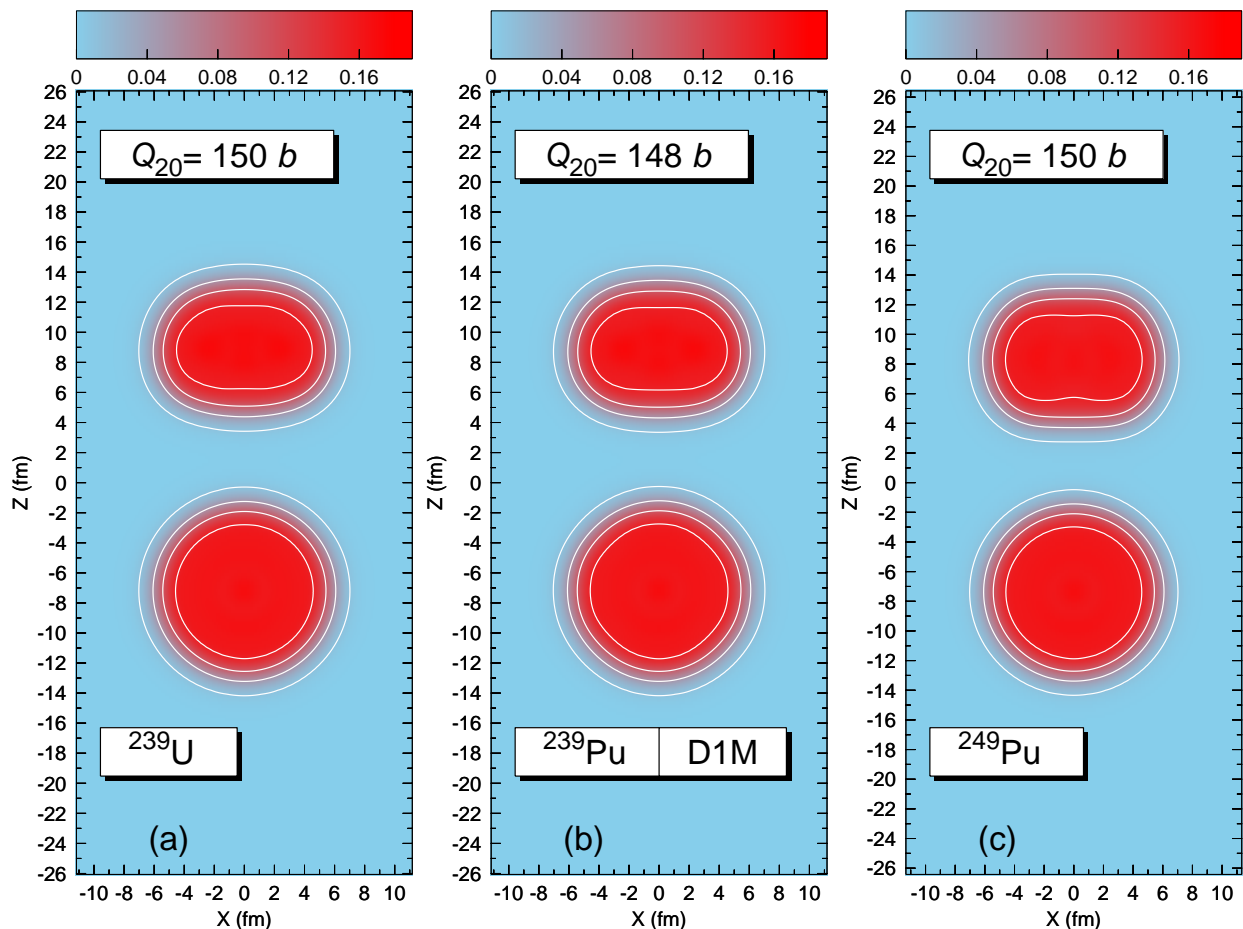


FIG. 10: (Color online) Density contour plots for the nuclei ^{239}U [panel (a)], ^{239}Pu [panel (b)] and ^{249}Pu [panel (c)]. The density profiles correspond to 2F solutions at the quadrupole deformations $Q_{20}=150$, 148 and 150 b. Densities are in units of fm^{-3} and contour lines are drawn at 0.01, 0.05, 0.10 and 0.15 fm^{-3} . For more details, see the main text.

statement is difficult to assess until a detailed calculation including particle number projection and fluctuations in the pairing gap are performed. On the other hand, it is satisfying to see that, in spite of the large variability in the predicted t_{SF} values with respect to the details involved in their computation, the main findings summarized in Fig. 8 still hold, i.e., regardless of the (ATD and/or GCM) scheme used as well as of the considered E_0 and/or η values our Gogny-D1M HFB-EFA calculations predict larger t_{SF} values for odd-mass U and Pu nuclei as compared with their even-even neighbors. On the other hand for both the U and Pu isotopic chains, we also observe a more pronounced competition between spontaneous fission and α -decay with increasing mass number A.

IV. SUMMARY AND CONCLUSIONS

In this paper, we have studied the fission properties of odd-mass U and Pu nuclei. To this end, we have considered isotopes in the mass range $A=233, \dots, 249$ as repre-

sentative samples. We have resorted to the constrained HFB-EFA in order to alleviate the already substantial computational effort required in the study of those odd-mass nuclear systems. Besides the usual constraints on both the proton \hat{Z} and neutron \hat{N} number operators, we have employed constraints on the axially symmetric quadrupole \hat{Q}_{20} , octupole \hat{Q}_{30} and \hat{Q}_{10} operators. On the other hand, HFB-EFA solutions corresponding to separated fragments have been reached with the help of constraints on the necking operator $\hat{Q}_{Neck}(z_0, C_0)$. We have presented a detailed account of the blocking methodology used to obtain 1F and 2F paths in the studied odd-mass nuclei. Zero-point quantum rotational and vibrational corrections have been added to the corresponding HFB-EFA energies *a posteriori*. The former has been computed in terms of the Yoccoz moment of inertia. On the other hand, both the GCM and ATD schemes have been used to obtain the collective masses and the vibrational corrections.

The systematic of the fission paths shows a rich topology for odd-mass U and Pu nuclei similar to the one already found in previous studies for even-even systems in

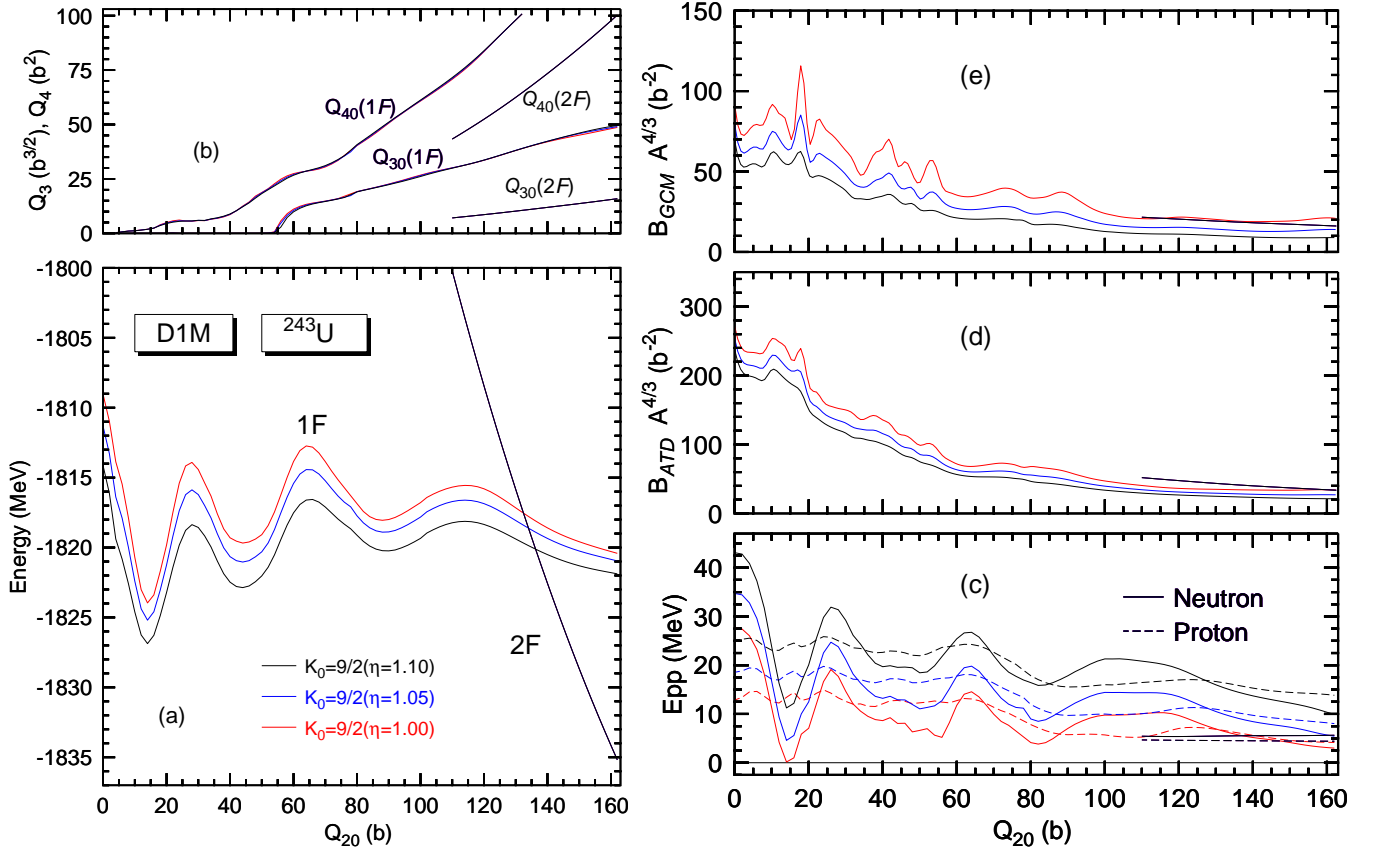


FIG. 11: (Color online) The $K_0 = 9/2$ HFB-EFA plus the zero point rotational energies obtained with the normal ($\eta=1.00$) and modified ($\eta=1.05$ and $\eta=1.10$) Gogny-D1M EDF are plotted in panel (a) as functions of the quadrupole moment Q_{20} for the nucleus ^{243}U . For each η value, both the one (1F) and two-fragment (2F) solutions are included in the plot. The octupole Q_{30} and hexadecapole Q_{40} moments corresponding to the 1F and 2F solutions are shown in panel (b). The pairing interaction energies are depicted in panel (c) for protons (dashed lines) and neutrons (full lines). The collective ATD and GCM masses are plotted in panels (d) and (e), respectively. For more details, see the main text.

this region of the nuclear chart [13–15]. Our Gogny-D1M calculations provide 1F paths with normal deformed, first and even second isomeric minima. In particular, those second fission isomers show up around ^{239}U and ^{243}Pu . We conclude that the shell effects leading to such second fission isomers are systematically present in our calculations for even-even and odd-mass U and Pu nuclei. Furthermore, the 1F paths display first and second barriers. Outer (third) barriers also emerge along the 1F paths as we move towards the very neutron-rich sectors in both the U and Pu chains. All those quantities exhibit odd-even effects as functions of the mass number A. We have found that, for the considered odd-mass nuclei, the ground state (1F and 2F) fission paths are always higher than the AV ones. This is a manifestation of the specialization energy arising from the fact that we have followed configurations with a fixed K_0 value. Those specialization energy effects together with the quenching of pairing correlations, taken into account selfconsistently via the Ritz-variational solution of the HFB-EFA equations, lead to larger spontaneous fission half-lives, computed within the WKB approximation, in odd-mass U and Pu

nuclei as compared with their even-even neighbors. We have found that α -decay is the dominant decay channel for most of the studied U and Pu nuclei. However, the steady increase in the α -decay lifetimes, as functions of the mass number A, leads to a pronounced competition with spontaneous fission.

We have studied the masses, charges and shapes of the fission fragments with the help of 2F HFB-EFA solutions at the largest quadrupole deformations. On the one hand, our results point to the key role played by the proton $Z=50$ and neutron $N=82$ shell closures in determining the properties of the predicted fission products. On the other hand, for several of the studied odd-mass U and Pu nuclei, we have obtained oblate deformed fission fragments that deserve further attention as they are usually assumed to be prolate.

We have studied the impact of pairing correlations on the spontaneous fission half-lives obtained for the considered odd-mass U and Pu systems. Our results, based on a modified Gogny-D1M EDF, reveal that increasing the strengths of the pairing fields by just 5 and 10 % lead to pronounced reductions of several orders of mag-

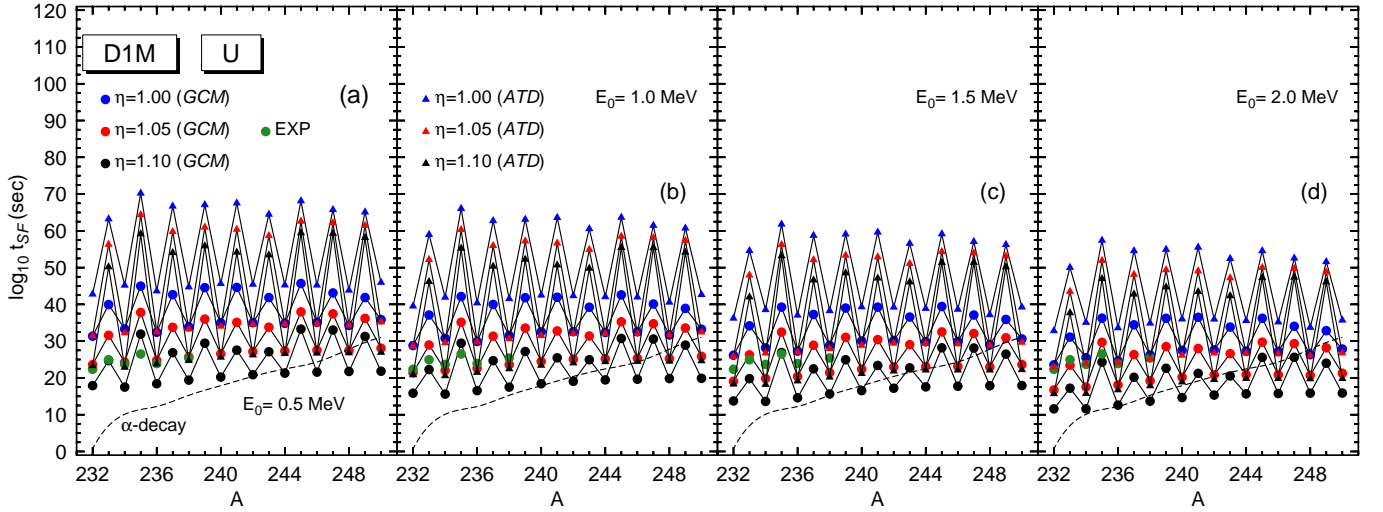


FIG. 12: (Color online) The spontaneous fission half-lives, predicted within the GCM and ATD schemes, for the isotopes $^{232-250}\text{U}$ are depicted as functions of the mass number A . Results have been obtained with the normal ($\eta = 1.00$) and modified ($\eta = 1.05$ and 1.10) Gogny-D1M EDF. Calculations have been carried out with $E_0 = 0.5$ [panel (a)], 1.0 [panel (b)], 1.5 [panel (c)] and 2.0 MeV [panel (d)], respectively. Results for even-even U isotopes are taken from Ref. [13]. The experimental t_{SF} values are taken from Ref. [53]. In addition, α -decay half-lives are plotted with short dashed lines. For more details, see the main text.

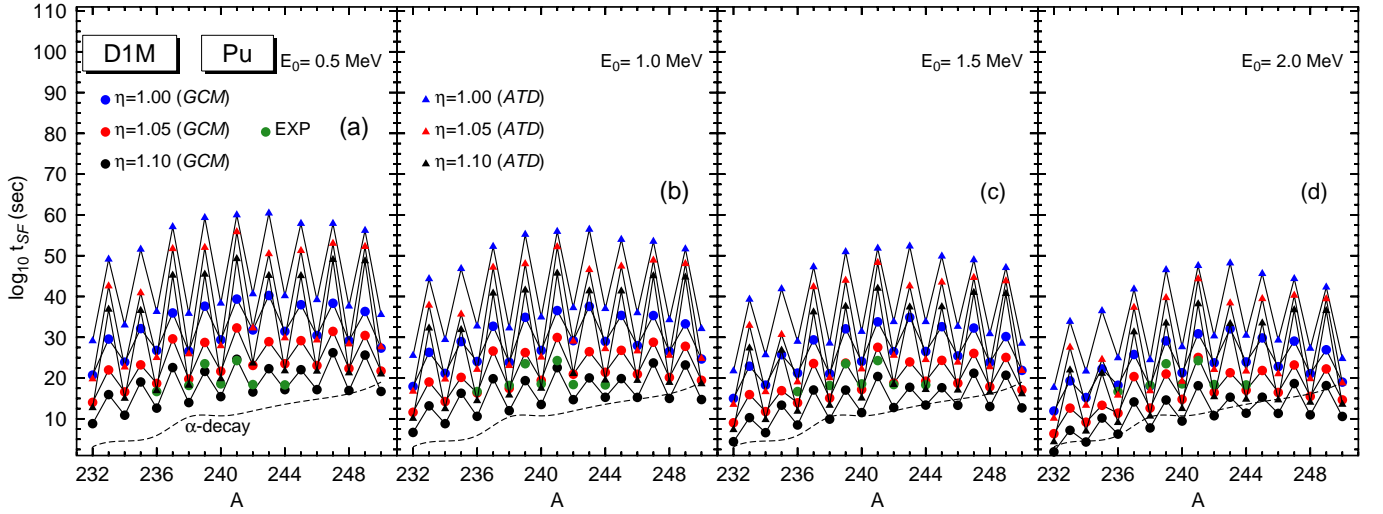


FIG. 13: (Color online) The spontaneous fission half-lives, predicted within the GCM and ATD schemes, for the isotopes $^{232-250}\text{Pu}$ are depicted as functions of the mass number A . Results have been obtained with the normal ($\eta = 1.00$) and modified ($\eta = 1.05$ and 1.10) Gogny-D1M EDF. Calculations have been carried out with $E_0 = 0.5$ [panel (a)], 1.0 [panel (b)], 1.5 [panel (c)] and 2.0 MeV [panel (d)], respectively. Results for even-even Pu isotopes are taken from Ref. [14]. The experimental t_{SF} values are taken from Ref. [53]. In addition, α -decay half-lives are plotted with short dashed lines. For more details, see the main text.

nitide in the t_{SF} values. Those results and the fact that at least for some of the considered odd-mass nuclei we are dealing with a weak pairing regime, call for a more sophisticated treatment of the (spontaneously broken) $U(1)$ particle number symmetry in which pairing fluctuations and their coupling to the relevant deformations are taken into account via the minimization of the action Eq. (4) [26]. Nevertheless, in spite of the strong variance of the predicted fission rates with respect to the details involved

in their computation, it is satisfying to observe the robustness in the systematic of the predicted t_{SF} values.

Finally, let us mention that the results discussed in this paper represent a first step towards a description of the fission properties of even-even and odd-mass U and Pu nuclei on an equal footing. A long list of tasks remains to be undertaken in the near future. For example, in addition to a more realistic treatment of pairing correlations, several aspects related with the computation of the col-

lective masses as well as the impact of triaxiality in some sectors of the 1F paths obtained for odd-mass U and Pu nuclei remain to be clarified. Work along these lines is in progress and will be reported elsewhere.

Acknowledgments

The work of LMR was partly supported by Spanish MINECO grant Nos FPA2015-65929 and FIS2015-63770.

-
- [1] S. Björnholm and J.E. Lynn, *Rev. Mod. Phys.* **52**, 725 (1980).
- [2] H.J. Specht, *Rev. Mod. Phys.* **46**, 773 (1974).
- [3] L. Meitner and O. R. Frish, *Nature* **143**, 239 (1939).
- [4] C. Wagemans, *The Nuclear Fission Process* (CRC Press, Boca Raton, 1991).
- [5] A. Baran, M. Kowal, P. -G. Reinhard, L. M. Robledo, A. Staszczak and M. Warda, *Nucl. Phys. A* **994**, 442 (2015).
- [6] N. Schunck and L. M. Robledo, *Rep. Prog. Phys.* **79**, 116301 (2016).
- [7] M. Bender, K. Rutz, P.-G. Reinhard, J.A. Maruhn and W. Greiner, *Phys. Rev. C* **58**, 2126 (1998).
- [8] M. Warda and J.L. Egidio, *Phys. Rev. C* **86**, 014322 (2012).
- [9] M. Warda, J. L. Egidio, L.M. Robledo and K. Pomorski, *Phys. Rev. C* **66**, 014310 (2002).
- [10] S. Ćwiok, P. -H. Heenen and W. Nazarewicz, *Nature* **433**, 705 (2005).
- [11] V.E. Viola Jr. and G.T. Seaborg, *J. Inorg. Nucl. Chem.* **28**, 741 (1966).
- [12] T. Dong and Z. Ren, *Eur. Phys. J. A* **26**, 69 (2005).
- [13] R. Rodríguez-Guzmán and L.M. Robledo, *Phys. Rev. C* **89**, 054310 (2014).
- [14] R. Rodríguez-Guzmán and L.M. Robledo, *Eur. Phys. J. A* **50**, 142 (2014).
- [15] R. Rodríguez-Guzmán and L.M. Robledo, *Eur. Phys. J. A* **52**, 12 (2016).
- [16] R. Rodríguez-Guzmán and L.M. Robledo, *Eur. Phys. J. A* **52**, 348 (2016).
- [17] S. A. Giuliani and L.M Robledo, *Phys. Rev. C* **88**, 054325 (2013).
- [18] M. Warda and L. M. Robledo, *Phys. Rev. C* **84**, 044608 (2011).
- [19] I. V. Panov, I. Yu. Korneev and F. -K. Thielemann, *Astron. Lett.* **34**, 189 (2008).
- [20] G. Martínez-Pinedo *et al*, *Prog. in Part. and Nucl. Phys.* **59**, 199 (2007).
- [21] S. A. Giuliani, G. Martínez-Pinedo and L. M. Robledo, arXiv/nucl-th/1704.00554 (2017).
- [22] H.J. Krappe and K. Pomorski, *Theory of Nuclear Fission*, *Lectures Notes in Physics*, **838** (Springer, Berlin, 2012).
- [23] P. Möller, A. J. Sierk, T. Ichikawa, A. Iwamoto and M. Mumpower, *Phys. Rev. C* **91**, 024310 (2015).
- [24] R. Julin, *Nucl. Phys. A* **834**, 15c (2010).
- [25] P. Ring and P. Schuck, *The Nuclear Many-Body Problem* (Springer, Berlin, 1980).
- [26] S. A. Giuliani, L.M Robledo and R. Rodríguez-Guzmán, *Phys. Rev. C* **90**, 054311 (2014).
- [27] J. F. Berger, M. Girod, and D. Gogny, *Nucl. Phys. A* **428**, 23c (1984).
- [28] J.-P. Delaroche, M. Girod, H. Goutte and J. Libert, *Nucl. Phys. A* **771**, 103 (2006).
- [29] N. Dubray, H. Goutte and J.-P. Delaroche, *Phys. Rev. C* **77**, 014310 (2008).
- [30] W. Younes and D. Gogny, *Phys. Rev. C* **80**, 054313 (2009).
- [31] N. Nikolov, N. Schunck, W. Nazarewicz, M. Bender and J. Pei, *Phys. Rev. C* **83**, 034305 (2011).
- [32] J.D. McDonnell, W. Nazarewicz and J.A. Sheikh, *Phys. Rev. C* **87**, 054327 (2013).
- [33] J. Erler, K. Langanke, H.P. Loens, G. Martínez-Pinedo and P.-G. Reinhard, *Phys. Rev. C* **85**, 025802 (2012).
- [34] A. Staszczak, A. Baran, W. Nazarewicz, *Physical Review C* **87**, 024320 (2013).
- [35] A. Baran, K. Pomorski, A. Lukasiak and A. Sobczewski, *Nucl. Phys. A* **361**, 83 (1981).
- [36] M. Baldo, L.M. Robledo, P. Schuck and X. Viñas, *Phys. Rev. C* **87**, 064305 (2013).
- [37] H. Abusara, A.V. Afanasjev and P. Ring, *Phys. Rev. C* **82**, 044303 (2010).
- [38] H. Abusara, A.V. Afanasjev and P. Ring, *Phys. Rev. C* **85**, 024314 (2012).
- [39] B.-N. Lu, E.-G. Zhao and S.-G. Zhou, *Phys. Rev. C* **85**, 011301 (2012).
- [40] S. Karatzikos, A. V. Afanasjev, G. A. Lalazissis and P. Ring, *Phys. Lett. B* **689**, 72 (2010).
- [41] I. Hamamoto, *Phys. Rev. C* **79** 014307 (2009).
- [42] S. Perez-Martin and L.M. Robledo, *Phys. Rev. C* **78**, 014304 (2008).
- [43] L. Bonneau, P. Quentin and P. Möller, *Phys. Rev. C* **76**, 024320 (2007).
- [44] T. Duguet, P. Bonche, P. -H. Heenen and J. Meyer, *Phys. Rev. C* **65**, 014310 (2001).
- [45] R. Rodríguez-Guzmán, P. Sarriguren, L.M. Robledo and S. Perez-Martin, *Phys. Lett. B* **691**, 202 (2010).
- [46] R. Rodríguez-Guzmán, P. Sarriguren and L.M. Robledo, *Phys. Rev. C* **82**, 044318 (2010).
- [47] R. Rodríguez-Guzmán, P. Sarriguren and L.M. Robledo, *Phys. Rev. C* **82**, 061302(R) (2010).
- [48] R. Rodríguez-Guzmán, P. Sarriguren and L.M. Robledo, *Phys. Rev. C* **83**, 044307 (2011).
- [49] N. Schunck *et al.*, *Phys. Rev. C* **81**, 024316 (2010).
- [50] P. Olbratowski, J. Dobaczewski, J. Dudek and W. Plóciennik, *Phys. Rev. Lett.* **93**, 052501 (2004).
- [51] J. Dechargé and D. Gogny, *Phys. Rev. C* **21**, 1568 (1980).

- [52] L.M. Robledo and G. F. Berstch, *Phys. Rev. C* **84**, 014312 (2011).
- [53] N. E. Holden and D. C. Hoffman, *Pure Appl. Chem.* **72**, 1525 (2000).
- [54] P. Fong, *Phys. Rev. C* **122**, 1545 (1961).
- [55] M. Brack, J. Damgaard, A.S. Jensen, H.C. Pauli, V.M. Strutinsky and C.Y. Wong, *Rev. Mod. Phys.* **44**, 320 (1972).
- [56] J.F. Berstch and H. Flocard, *Phys. Rev. C* **43**, 2200 (1991).
- [57] S. Goriely, S. Hilaire, M. Girod and S. Péru, *Phys. Rev. Lett.* **102**, 242501 (2009).
- [58] J. Dechargé and D. Gogny, *Phys. Rev. C* **21**, 1568 (1980).
- [59] R. Rodríguez-Guzmán, L.M. Robledo and P. Sarriguren, *Phys. Rev. C* **86**, 034336 (2012).
- [60] L.M. Robledo and R. Rodríguez-Guzmán, *J. Phys. G: Nucl. Part. Phys.* **39**, 105103 (2012).
- [61] R. Rodríguez-Guzmán, L.M. Robledo, P. Sarriguren and J. E. García-Ramos, *Phys. Rev. C* **81**, 024310 (2010).
- [62] L.M. Robledo, R. Rodríguez-Guzmán, and P. Sarriguren, *J. Phys. G: Nucl. Part. Phys.* **36**, 115104 (2009).
- [63] M. Gaudin, *Nucl. Phys.* **15**, 89 (1960).
- [64] S. Perez-Martin and L.M. Robledo, *Phys. Rev. C* **76**, 064314 (2007).
- [65] C. Titin-Schnaider and Ph. Quentin, *Phys. Lett. B* **49**, 213 (1974).
- [66] R. Rodríguez-Guzmán, J.L. Egido and L.M. Robledo, *Phys. Lett. B* **474**, 15 (2000).
- [67] R. Rodríguez-Guzmán, J.L. Egido and L.M. Robledo, *Phys. Rev. C* **62**, 054308 (2000).
- [68] J.L. Egido and L.M. Robledo, *Lectures Notes in Physics* **641**, 269 (2004).
- [69] M. Baranger and M. Veneroni, *Ann. Phys.* **114**, 123 (1978).
- [70] H.M. Sommermann, *Ann. Phys.* **151**, 163 (1983).
- [71] P. Ring, L.M. Robledo, J.L. Egido and M. Faber, *Nucl. Phys. A* **419**, 261 (1984).
- [72] M. Girod and B. Grammaticos, *Nucl. Phys. A* **330**, 40 (1979).
- [73] M.J. Giannoni and P. Quentin, *Phys. Rev. C* **21**, 2060 (1980).
- [74] M.J. Giannoni and P. Quentin, *Phys. Rev. C* **21**, 2076 (1980).
- [75] J. Libert, M. Girod and J.P. Delaroche, *Phys. Rev. C* **60**, 054301 (1999).
- [76] A. Baran, *Phys. Lett. B* **76**, 8 (1978).
- [77] A. Baran, J. A. Sheikh, J. Dobaczewski, W. Nazarewicz and A. Staszczak, *Phys. Rev. C* **84**, 054321 (2011).
- [78] M. Kowal and J. Skalski, *Phys. Rev. C* **85**, 061302(R) (2012).
- [79] P. Jachimowicz, M. Kowal and J. Skalski, *Phys. Rev. C* **87**, 044308 (2013).
- [80] V. V. Pashkevich, *Nucl. Phys. A* **169**, 275 (1971).
- [81] P. Möller, *Nucl. Phys. A* **192**, 529 (1972).
- [82] K. Rutz, J. Mahrun, P. -G. Reinhard and W. Greiner, *Nucl. Phys. A* **590**, 680 (1995).
- [83] J. F. Berger, M. Girod and D. Gogny, *Nucl. Phys. A* **502**, 85 (1989).
- [84] J. Zhao, B. -N. Lu, D. Vretenar, E. -G. Zhao and S. -G. Zhou, *Phys. Rev. C* **91**, 014321 (2015).
- [85] N. Nenoff, P. Bringel, A. Bürger, S. Chmel, S. Dababneh, M. Heil, H. Hübel, F. Käppeler, A. Neusser-Neffgen and R. Plag, *Eur. Phys. J. A* **32**, 165 (2007).
- [86] G. M. Ter-Akopian, J. H. Hamilton, Yu. Ts. Oganessian, A. V. Daniel, J. Kormicki, A. V. Ramayya, G. S. Popeko, B. R. S. Babu, Q.-H. Lu, K. Butler-Moore, W. -C. Ma, S. Ćwiok, W. Nazarewicz, J. K. Deng, D. Shi, J. Kliman, M. Morhac, J. D. Cole, R. Aryaeinejad, N. R. Johnson, I. Y. Lee, F. K. McGowan and J. X. Saladin, *Phys. Rev. Lett.* **77**, 32 (1996).
- [87] M. Piessens, E. Jacobs, S. Pommé and D. D. Frenne, *Nucl. Phys. A* **556**, 88 (1993).
- [88] L. Dematté, C. Wagemans, R. Barthélémy, R. Dhont and A. Deruytter, *Nucl. Phys. A* **617**, 331 (1997).
- [89] D.C. Hoffman and M.M. Hoffman, *Ann. Rev. Nucl. Sci.* **24**, 151 (1974).
- [90] H. Goutte, J. F. Berger, P. Casoli and D. Gogny, *Phys. Rev. C* **71**, 024316 (2005).
- [91] B. D. Wilkins, E. P. Steinberg and R. R. Chasman, *Phys. Rev. C* **14**, 1832 (1976).
- [92] Brookhaven National Nuclear Data Center, <http://www.nndc.bnl.gov/nudat2>
- [93] K.-H. Schmidt et al., *Nucl. Phys. A* **665**, 221 (2000).
- [94] P. Möller and A. Iwamoto, *Phys. Rev. C* **61**, 047602 (2000).
- [95] P. Möller, D.G. Madlan, A.J. Sierk and A. Iwamoto, *Nature* **409**, 785 (2001).